# 3D Bioprinted Cell-laden GrooveNeuroTube: A Multifunctional Platform for *Ex Vivo* Neural Cell Migration and Growth Studies

*Jagoda Litowczenko[1*], Yannick Richter[2], Hawrez Ismael[1], Łukasz Popenda[3], Adam Ostrowski[4], Katarzyna Fiedorowicz[4], Jose Carlos Rodrigez Cabello[5], Jacek K. Wychowaniec[6], Krzysztof Tadyszak[7]*

[1]Center for Advanced Technologies, Adam Mickiewicz University in Poznań, Uniwersytetu Poznańskiego 10, 61-614 Poznań, Poland

[2]Department of Chemistry and Chemical Biology, TU Dortmund University, Dortmund 44227, Germany

[3]NanoBioMedical Centre, Adam Mickiewicz University, Wszechnicy Piastowskiej 3, 61614 Poznań, Poland

[4]Institute of Molecular Physics, Polish Academy of Sciences, Smoluchowskiego 17, 60-179 Poznań, Poland

[5]BIOFORGE Lab, LADIS, University of Valladolid, CIBER-BBN, Valladolid, Spain

[6]AO Research Institute Davos, Clavadelerstrasse 8, 7270, Davos, Switzerland

[7]Institute of Macromolecular Chemistry, CAS, Heyrovského nám. 2, 162 06 Prague 6, Czech Republic

**The correspondence** should be addressed to Jagoda Litowczenko.: Phone: +48511002320; e-mail: jagoda.litowczenko@amu.edu.pl

## Graphical abstract:

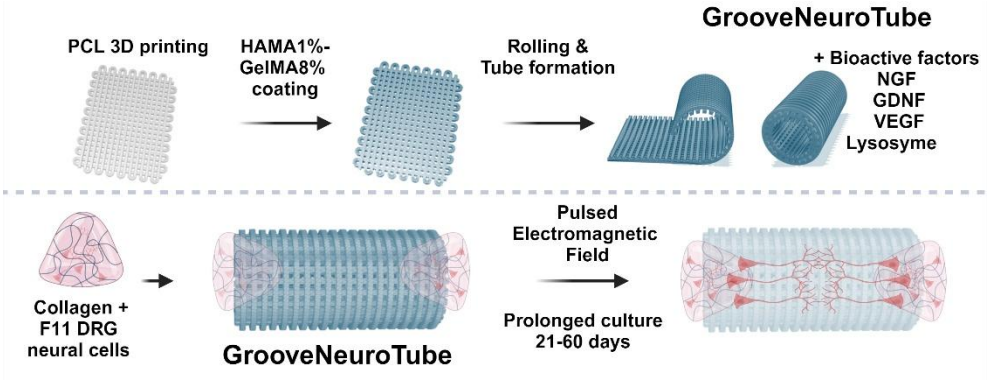


Graphical abstract

The graphical abstract was created with BioRender.com.

**Abstract**

Extensive peripheral nerve injuries often lead to the loss of neurological function due to slow regeneration and limited recovery over large gaps. Current clinical interventions, such as nerve guidance conduits (NGCs), face challenges in creating biomimetic microenvironments that effectively support nerve repair. The developed ***GrooveNeuroTube*** is composed of hyaluronic acid methacrylate and gelatin methacrylate hydrogel, incorporating active agents (growth factors and antibacterial agents) encapsulated within an NGC conduit made of 3D-printed PCL grid fibers. In vitro studies showed that ***GrooveNeuroTube*** significantly promoted migration of dorsal root ganglion (DRG) neuronal cells, 3D bioprinted at the far ends of the conduit to imitate a proximal nerve injury as a novel *ex vivo* model. A long-term culture of up to 60 days was employed to better mimic *in vivo* conditions. This model tested the effects of pulsed electromagnetic field (PEMF) stimulation on neural tissue development. After 60 days, ***GrooveNeuroTube*** showed a 32% cell migration increase compared to the growth-factor-group and 105% compared to the no-growth-factor condition. These results confirm that the ***GrooveNeuroTube*** system can effectively support sustained neural cell migration and maturation over extended periods, proving a new technology for testing peripheral nerve injury *ex vivo*.

**Keywords:** nerve guidance conduits, 3D bioprinting; neurite outgrowth; neural migration; hyaluronic acid; gelatin methacrylate

## 1. Introduction

Extensive peripheral nerve injuries (PNI) represent a significant clinical challenge, often leading to substantial functional deficits and prolonged recovery due to the limited capacity for repair.[1, 2] Although the peripheral nervous system (PNS) possesses some regenerative abilities, clinical outcomes following PNI remain suboptimal, highlighting the necessity for

advanced therapeutic strategies. Severe PNIs, particularly those with segmental nerve defects exceeding 4 cm, present additional complexities as direct end-to-end repair generates detrimental tension, hindering recovery.[3] In such cases, nerve grafts or conduits designed to bridge the gap have become a cornerstone and necessity of nerve repair. Autologous nerve grafting, considered the gold standard, is still widely employed but is associated with several drawbacks, including donor site morbidity, size mismatches, and the limited availability of donor nerves.[4] As an alternative, nerve guidance conduits (NGCs) constructed from biomaterials have gained significant attention.[1] These conduits can be made from natural materials like collagen, which offer biocompatibility,[5] or synthetic materials like polycaprolactone (PCL), which allow tuneable mechanical and degradation properties.[6] Furthermore, integrating advanced technologies, such as topographical patterning or the addition of bioactive agents, can enhance axonal alignment and nerve regeneration.[4, 6, 7] Topographical patterns can be especially suitable in neural tissue engineering to produce neural conduits to enhance axonal growth and nerve regeneration. Axon outgrowth and pathfinding are crucial for re-establishing neuronal circuitry in re-wiring damage from neuronal injury.[8-11] Biofabrication technologies enable rapidly developing more complex NGCs with custom designs and hierarchical arrangements that can leverage individual requirements for future personalized approaches.[12]

Hyaluronic acid (HA) is a biocompatible and biodegradable glycosaminoglycan found in the extracellular matrix [13] known for its moisture retention, immunomodulatory properties,[14] and gel-like characteristics that support tissue regeneration.[15-18] It plays a critical role in cell adhesion, proliferation, and wound healing, making it valuable for neural tissue engineering (NTE).[19] HA-based hydrogels have been shown to promote neuronal outgrowth and differentiation, offering the potential to treat neurodegenerative disorders.[19]

Studies have demonstrated that HA hydrogels enhance neural cell survival, influence neural patterning, and improve neurological function by releasing neurotrophic factors, making them promising for CNS injury treatment.[19] Soft HA hydrogels, in particular, significantly enhance neurite outgrowth and neural differentiation compared to stiffer alternatives.[19] Encapsulation of human embryonic stem cell-derived neural stem cells (hESC-NSCs) within HA hydrogels improves cell viability and differentiation after spinal cord injury (SCI) while reducing cavity formation and glial scarring.[19] Additionally, HA-based electrospun scaffolds, such as HA/heparin nanofibers, accumulate growth factors like bFGF and NGF, promoting neuronal differentiation and enhancing cell proliferation.[20]

Gelatin is a denatured protein derived from collagen through acidic (type A) or alkaline (type B) hydrolysis.[21] Its properties vary depending on the collagen source, animal age, and processing methods.[22, 23] Gelatin provides a biocompatible environment that supports cell adhesion, growth, and differentiation, making it widely used in tissue engineering.[24-27] It is water-soluble and undergoes reversible gelation in response to temperature changes.[28] However, gelatin scaffolds can lose their structure in aqueous environments, necessitating modifications to improve their mechanical and thermal stability.[28, 29]

Gelatin-based hydrogels have shown great promise in neural tissue engineering, supporting the growth and viability of neural cells in 3D cultures.[19] Studies have demonstrated that gelatin scaffolds offer appropriate stiffness and stability, promoting cell proliferation and making them promising candidates for CNS repair and regeneration.[30]

Hydrogels have become materials capable of mimicking the tissue microenvironment, enabling controlled growth factor delivery, and being patternable for fabrication into desired constructs.[31] In the context of spinal cord and PNI, gelatin methacrylate (GelMA) has shown significant promise.[32] Recent studies have demonstrated using GelMA-based hydrogels in digital light processing (DLP) 3D printing to fabricate multichannel NGCs for peripheral nerve

regeneration.[30] These GelMA-based NGCs provided an excellent environment for neural PC12 cells, supporting their survival, proliferation, and directional migration along the longitudinal channels. Furthermore, neural crest stem cells (NCSCs) cultured on the printed GelMA-NGCs were able to differentiate into neurons, highlighting the potential of GelMA-based NGCs in neural tissue engineering.

F11 DRG neural cells, derived from neonatal rat dorsal root ganglia (DRG) neurons fused with the mouse neuroblastoma cell line N18Tg2, serve as an established *in vitro* model for replicating features of injured peripheral neurons.[33] These cells exhibit peripheral sensory neuron characteristics, including a wide array of ion channels and specific neuronal markers, and are widely used to study signalling and neurite outgrowth. Their responsiveness to electromagnetic stimulation makes them ideal for exploring regenerative mechanisms. F11 cells have been employed in studies of neuronal plasticity and transcriptional regulation during PNS repair.

In material-based approaches, F11 cells have been exposed to pulsed electromagnetic fields (PEMFs) produced by a custom-made device.[34] By modulating parameters such as frequency, pulse repetition frequency, and duty cycle, optimal conditions for enhancing cell viability and neurite outgrowth were identified.[34] PEMFs have been shown to promote neural regeneration in F11 cells by accelerating neurogenesis, as confirmed by gene expression analysis 10 days post-stimulation.[34] Recent studies also demonstrate the protective effects of low-frequency, low-energy PEMFs on neuron-like and microglial cells under inflammation- and hypoxia-induced injury conditions.[35] In neuron-like cells (e.g., SH-SY5Y and PC12), PEMF exposure reduced hypoxia-induced damage by lowering cell death and oxidative stress. In microglial N9 cells, PEMF treatment decreased the release of pro-inflammatory cytokines (TNF-α, IL-1β, IL-6, IL-8) after lipopolysaccharide (LPS) stimulation, suggesting both neuroprotective and anti-inflammatory effects. These findings position PEMFs as a promising

strategy for promoting neural regeneration and mitigating ischemic injury, potentially offering new translational approaches combining grafting with external field control in patients.

GelMA synthesized from type A gelatin has been shown to have no immunogenic effects on surrounding neural tissues *in vitro* and *ex vivo*.[32] While hyaluronic acid (HA) is widely used in neural tissue engineering, its application in neural conduits is relatively unexplored. In this study, we report the first combination of HAMA-GelMA hydrogels with growth factors to enhance the migration of neural cells. Additionally, the significant limitations of HAMA and GelMA, such as poor mechanical properties, were overcome by incorporating a unique 3D-printed polycaprolactone (PCL) fiber grid architecture. Hence, in this study, we fabricated a GrooveNeuroTube, incorporating 3D-printed PCL fibers and a composite HAMA-GelMA hydrogel loaded with bioactive agents (neural growth factor - NGF, glial cell line-derived neurotrophic factor - GDNF, vascular endothelial growth factor – VEGF, and lysozyme). The surface of PCL fibers was engineered with a specific micro-topography to guide neural cells and maintain conduit integrity. We hypothesized that the developed conduit, consisting of overlapping PCL fibers and an interconnected HAMA-GelMA hydrogel network, can significantly enhance the growth and migration of 3D bioprinted neural DRG cells, offering a promising strategy for nerve regeneration. For that, we utilized 3D bioprinting technology to mimic neural stumps, which require the placement of a neural conduit to enhance neural cell migration for regeneration. The cell-laden hydrogel, 3D bioprinted on both sides of the neural conduit, was cultured under prolonged conditions for 1 to 60 days to investigate the migration dynamics within the developed ***GrooveNeuroTube***. Furthermore, we specifically targeted the design of this conduit to support DRG F11 neuronal cell migration and neurite extension over prolonged periods, providing a new platform for ex vivo-like studies. Exemplary, we investigated in this model the synergistic effect of PEMF stimulation on neural regeneration,

159 hypothesizing that the combined approach of bioengineered graft would significantly enhance
160 cellular alignment, proliferation, and axonal growth.
161
162 **2. Materials and Methods**
163 **2.1. PCL preparation**
164 Polycaprolactone (PCL, Sigma Aldrich) pellet with a molar mass of $M_n$ = 80 kDa was used for
165 3D printing.
166 **2.2. 3D printing**
167 *3D printing:* Cellink Bio X2 - 3D printer (CellInk, Gothenburg, Sweden) was used for the PCL
168 3D printing. 33 mm (length) x 16.5 mm (width) rectangular constructs consisting of 2 layers
169 of fibers were printed by pneumatic extrusion print head at a temperature of 90 °C. The
170 optimization phase consisted of testing various printing temperatures (90 °C to 220 °C),
171 different pressures (175–550 kPa), and printing speeds (10–15 mm/s), after which the
172 following final printing parameters were selected for biological studies: 90°C, 180 kPa, and
173 two printing speeds: 10 mm/s and 15 mm/s. For the 3D printing of the PCL, we used an
174 aluminum cartridge and a metal nozzle with a pressure of 180 kPa to print directly onto a glass
175 petri dish. After 3D printing, constructs were left to cool down at room temperature before
176 being carefully removed. A 3D-printed PCL scaffold with dimensions of 33 mm (length) ×
177 16.5 mm (width) was tightly rolled three times along its shorter side to form a tube with
178 dimensions of 16.5 mm x approximately 7.5 mm (see ***Figure 1*** in the main text for more
179 details). To secure the tube and prevent it from unrolling, a connecting section of the sheet was
180 manually bonded to the tube by applying additional PCL fibers using the thermoplastic
181 printhead of the BioX2, heated to 60°C.
182 **2.3. Composite Hydrogel preparation**

183 Methacrylated Gelatin (GelMA) powder with a high degree of methacrylation (DoM = 95%,
184 PhotoGel® Catalog #5273, Advanced BioMatrix, Inc.) was dissolved in PBS preheated to 60°C
185 and placed in a water bath with shaking for approximately 40 minutes until fully dissolved. For
186 different experiments, hydrogels were prepared by dissolving GelMA powder in 1X PBS at 5,
187 10 or 15% (w/v) at 60°C with 37.4 mg/mL ruthenium photoinitiator and 119 mg/mL of sodium
188 persulfate. Hydrogels were sterilized through a 0.2 µm syringe filter (83.1826.102, Starstedt).
189 Hydrogels were photopolymerized using a 405 nm diode source (from Cellink BioX2) for 45
190 s (with power irradiation determined as 5.3 W at a 1 cm distance from hydrogel). Methacrylated
191 Hyaluronic Acid (DoM = 45-65%, HAMA, PhotoHA®-Stiff Catalog #5275, Advanced
192 BioMatrix, Inc.) powder with was added to cooled PBS (4°C) and left overnight in a
193 refrigerator on a rotator to ensure complete dissolution. Once the GelMA solution was fully
194 dissolved, it was cooled to 24°C. Meanwhile, the HAMA solution was warmed to 24°C and
195 then combined with the GelMA solution using a positive displacement pipette. The mixture
196 was placed on a rotor in a $CO_2$ incubator at 37°C for 30 minutes to form a uniform HAMA-
197 GelMA suspension with 37.4 mg/mL ruthenium photoinitiator and 119 mg/mL of sodium
198 persulfate. The concentrations of GelMA and HAMA were chosen such that the final
199 concentrations of GelMA were 4, 8, or 10 w/v%, whilst the HAMA concentration was fixed at
200 1 w/v%. The preparation of the key hydrogel formulation used throughout manuscript is
201 presented at ***Figure 1A***: Hyaluronic acid methacrylate (HAMA, 1 w/v%) is combined with
202 gelatin methacrylate (GelMA, 8 w/v%) to produce the composite hydrogel, referred to as
203 HAMA1%-GelMA8%. For other concentrations, the number in GelMA is simply updated in
204 sample naming. In some cases, as described in the main text, the following bioactive
205 compounds were added to the HAMA1%-GelMA8% composite at the mixing stage on a rotor
206 in a $CO_2$ incubator at 37°C for 30 minutes: Nerve growth factor (NGF) at 5 ng/mL, Glial cell

207 line-derived neurotrophic factor (GDNF) at 10 ng/mL, and Vascular endothelial growth factor
208 (VEGF) at 50 ng/mL, along with lysozyme at 0.5 mg/mL.

209 **2.4. Production of porous GroveNeuroTube - HAMA-GelMA 3D PCL tubes:** To fabricate
210 the composite HAMA-GelMA-PCL, a 3D-printed PCL grid with dimensions of 33 mm x 16.5
211 mm was laid flat in a Petri dish. Next, a preheated (to 24°C) solution of HAMA1%-GelMA8%
212 was injected into the center of the PCL grid, allowing the solution to evenly distribute across
213 the grid. At this stage, photopolymerization was initiated by exposing the hydrogel to a 405 nm
214 diode light source (Cellink BioX2) for 45 seconds, with a power irradiation of 5.3 W at a 1 cm
215 distance. Subsequently, the composite hydrogel containing the PCL was tightly rolled three
216 times to form a tube measuring 16.5 mm in length and 5 mm in diameter, similarly to the
217 protocol described above for PCL alone. To secure the structure and prevent unrolling, a
218 connecting section of the sheet was again bonded to the tube by applying PCL fibers using the
219 thermoplastic printhead of the BioX2, heated to 60°C. Once completely rolled, the tube was
220 allowed to air-dry for 1 hour (***Figure 1B, C***). HAMA1%-GelMA8% containing growth factors
221 (abbreviated as HAMA1%-GelMA8%-GF) was only added once the tube cooled down to
222 37°C.

223 **2.5. Scanning electron microscopy (SEM)**

224 The morphology of all samples was analysed using an SEM-7001TTLS microscope (JEOL
225 Ltd., Akishima, Japan) operated at an accelerating voltage of 15 kV. Hydrogels with 5, 8, and
226 10% GelMA concentrations were further examined using the same SEM coupled with a
227 PP3000T cryo-preparation system (Quorum Technologies, Laughton, UK). This setup enabled
228 the preparation, processing, and transfer of cryo-fixed specimens directly into the SEM
229 chamber for observation in a vitrified state. The samples were mounted on metal holders and
230 rapidly cryo-fixed by immersion in sub-cooled liquid nitrogen ($N_2$ slush) at −210 °C. The
231 frozen samples were then transferred under vacuum into the SEM preparation chamber,

maintained at −180 °C. Within this chamber, the specimens were fractured to reveal fresh inner surfaces, sublimated to remove surface ice, and coated with a thin layer of platinum. Subsequently, the samples were transferred under vacuum to the SEM cryo-stage, maintained at −190 °C, where imaging of the surfaces was performed. Additionally, elemental analysis of the cryo-prepared hydrogels was conducted at an accelerating voltage of 15 kV. Pore size analysis was performed on over 400 pores using ImageJ.

**2.6. Fourier transform infrared spectroscopy (FTIR)**

FTIR measurements were performed at room temperature between 400-4000 $cm^{-1}$ using a Nicolet iS50 FT-IT spectrophotometer (Thermo Scientific, Waltham, United States). The HAMA1%, GelMA8%, HAMA1%-GelMA8%, and crosslinked HAMA1%-GelMA8% freeze-dried samples were placed onto the ATR crystal and pressed down to ensure contact between the sample and the crystal. The measurements were taken with a resolution of 4 $cm^{-1}$ and for 64 scans.

**2.7. Nuclear Magnetic Resonance (NMR)**

To study the crosslinking process, $^{1}H$ NMR spectra were recorded using an Agilent DD2 800 spectrometer (Agilent Technologies, Santa Clara, CA, USA) equipped with a 5 mm 1H/13C/15N probe. Measurements were conducted at 37 °C with $D_2O$ as the solvent. The sample concentration was maintained at 80 mg/mL of GelMA (8%), 10 mg/mL of HAMA 1%, 0.18 mg/mL of ruthenium photoinitiator, and 0.56 mg/mL of sodium persulfate. The sample was exposed to UV light directly in an NMR tube to induce crosslinking. $^{1}H$ NMR experiments were performed using Agilent's standard pulse sequence with a low-power pre-saturation pulse for residual water suppression. To enhance the signal-to-noise ratio, 128 scans were accumulated per spectrum. The spectra were referenced relative to 3-(Trimethylsilyl)propionic acid-$d_4$ sodium salt (TSP) as an external standard.

**2.9 Degradation and swelling**

To evaluate the in vitro degradation behavior of the hybrid 3D conduit composed of 3D-printed PCL mesh and photocrosslinked hydrogel (GelMA 8% w/v and HAMA 1% w/v), we conducted a longitudinal mass loss analysis under simulated physiological conditions. Cylindrical constructs (length 16.5 mm, outer diameter 7.5 mm) were fully immersed in phosphate-buffered saline (PBS) and incubated at 37°C in a 5% $CO_2$ atmosphere. The constructs (n = 3) were first weighed (analytical balance) at day 0 and subsequently re-weighed at 3, 7, 14, 28, and 60 days following removal, PBS removal, and drying (blotting + short desiccation).

The swelling capacity (S%) was determined using gravimetric method. Initially, the dry weigh of each sample ($W_o$) was measured followed by immersion of the samples in 10 mL of Milli-Q water and retrieved at predetermined intervals upto 720 min. After removal, excess surface water was gently blotted with moistened filter paper and the samples were weighed again ($W_f$). The swelling capacity was calculated using equation (1)

$$S\ (\%) = \left(\frac{Wf - Wo}{Wo}\right) * 100$$

**2.9. Rheological measurements**

The storage (G') and loss (G") moduli of the hydrogels were measured using an TA Instruments AR 2000ex rheometer equipped with a 12 mm diameter top plate and a 1 mm gap in a parallel plate geometry. For sample preparation, 500 µL of hydrogel was photopolymerized in a specially designed ceramic mould with wells measuring 20 mm in diameter and 10 mm in height, sealed at the bottom with a removable PDMS layer. The samples were carefully transferred onto the stationary bottom plate of the rheometer using a spatula, ensuring minimal disturbance to the sample structure. The top plate was gradually lowered to avoid disrupting the hydrogel. Before each measurement, the sample was equilibrated at 37 °C for 3 minutes. Strain sweeps were performed from 1% to 10% strain at a fixed frequency of 1 Hz, and

281 frequency sweeps were conducted from 1 Hz to 20 Hz at a constant strain of 1% within the
282 linear viscoelastic region. Measurements included G', G" and complex viscosity |η*|. Each
283 measurement was repeated three times to ensure reproducibility.

284 **2.10. Cell Culture:** Immortalized Dorsal Root Ganglion Neuron Cell Line (F11 cell line from
285 rat, 08062601, ECACC) were purchased from Merck and cultured in DMEM + 2mM
286 Glutamine + 10% Foetal Bovine Serum (FBS). The medium was supplemented with penicillin
287 (100 U/mL) and streptomycin (100 mg/mL), and F11 were cultured at 37°C in a humidified
288 atmosphere of 5% $CO_2$. Cells were grown in sterile 25 $cm^2$ and 75 $cm^2$ tissue culture flasks.
289 When cells reached 80% confluence, they were transferred and sub-cultured in a new flask by
290 trypsinization with 0.05% trypsin. Cell growth and confluence were observed under the light
291 microscope and counted by an Automated Cell Counter (BioRad). Experiments were carried
292 out with cells from the third to sixteen passages.

293 **2.11. DRG neuronal cells seeding prior to microscopies imaging:** PCL fibers pattern
294 matrices were sterilized by 70% ethanol washing followed by subsequent 30 min UV light
295 exposure (λ=254 nm). Samples were exposed to 1 hour of UV light exposure and placed in
296 sterile multi-well plates. After reaching 80% confluency, the F11 cells were washed with
297 Dulbecco's Phosphate Buffered Saline containing no calcium, magnesium, or phenol red (D-
298 PBS, ThermoFisher, 12604-013) and collected by trypsinization at 37 °C for 5 minutes. Cells
299 were counted by Automated Cell Counter (BioRad). Dissociated F11 cells were plated onto
300 PCL grids at a density of $25 \times 10^4$ cells per $cm^2$. The medium was replaced at 3 days post-
301 seeding and then refreshed every 3–4 days. Cells were grown in humidified conditions (95%
302 humidity) at 37°C and 5% $CO_2$.

303 **2.12. 3D bioprinting on GrooveNeuroTube – *ex vivo* model**

304 10X PBS or 10X culture medium chilled to 15 °C was combined with a
305 8 mg/mL methacrylated type I bovine collagen solution (PhotoCol®, Catalog #5198, Advanced

306 BioMatrix, Inc.)) chilled to 4 ºC in an 8:1 ratio under gentle swirling. The pH was carefully
307 adjusted to 7.0–7.5 using sterile 0.1 M NaOH and monitored with a pH meter or phenol red.
308 The volume was brought to 10 parts with sterile water, ensuring the mixture's temperature
309 remained between 2–10°C to prevent premature gelation. The mixture was then warmed to
310 37°C and allowed to form a gel over 90–120 minutes. For gels containing F11 DRG neural
311 cells, a 1:1 (v/v) mixture of a cell suspension (500,000 cells/mL) and collagen was prepared at
312 4 °C. Aliquots (0.5 mL) were placed into a 24-well plate, with one column left as a non-
313 crosslinked control, and microbial transglutaminase (TG) (3.33:1 collagen: TG w/w%) added
314 to the others. Plates were prepared for each time point and incubated under standard culture
315 conditions, and media changes were made every 3 days. Time-zero samples were analyzed
316 immediately after a 30-minute incubation. The pre-printed tube was used as a base for
317 bioprinting collagen. The bioink, consisting of F11 DRG neural cells pellet embedded in
318 collagen, was loaded into the bioprinter cartridge. Subsequently, 1 layer of this bio-ink of 500
319 µL of cell-laden (250,000 cells) collagen was deposited onto one end of the tube within 3
320 minutes at room temperature using a 20G cylindrical needle and pressure of 15 kPa. Afterward,
321 bioprinting of the equivalent volume of the bio-ink was performed on the opposite end of the
322 tube. The tubes were then placed horizontally in 6-well plates and incubated to allow mTG
323 crosslinking. After 30 minutes, medium was added to the wells, and a medium change was
324 performed the following day.

325 **2.13. Migration test – 3D cell bioprinting on both tube ends**

326 Migration within 3D tubes was evaluated using confocal microscopy and cell labeling. To
327 estimate cell viability and migration within the constructs, the Fluorescein Diacetate/Propidium
328 Iodide (FDA/PI) viability assay was employed. Constructs were sectioned into 500 µm
329 transverse slices using a vibratome at three time points: day 1 (at the gel corner), day 14, and
330 day 28 of culturing (from the central region) (as shown in main text in ***Figure 8***). Samples were

331 embedded in 6% agarose blocks (Condalab, 8017.00) and sectioned transversely at 500 µm
332 thickness using a vibratome (Leica VT100S). The sections were immersed in DMEM medium
333 without foetal calf serum (FCS), containing FDA (5 mg/mL) and PI (2 mg/mL), for 5 minutes.
334 Following incubation, the staining solution was removed, and the cross-sections were washed
335 twice with PBS. The samples were then placed in DMEM medium without FCS and
336 immediately observed using a IX 73 Olympus for live/dead imaging. The remaining constructs
337 were used for immunostaining. Constructs were fixed in 4% paraformaldehyde overnight at
338 4°C. The next day, tissues were washed three times for 30 minutes each with 1X PBS on a
339 rotary shaker. Samples were embedded in 6% agarose blocks (Condalab, 8017.00) and
340 sectioned transversely at 300 µm thickness using a vibratome (Leica VT100S). Sections were
341 incubated for 4 hours in blocking buffer (1X PBS, 0.5% Triton X-100, 1% BSA). Primary
342 antibodies were used to detect antigens: rabbit anti-Dcx (1:100, ThermoFisher), mouse anti-
343 Map2 (1:250, ThermoFisher), and rabbit anti-Syp (1:100, Abcam). After PBS washing,
344 secondary antibodies such as Donkey anti-mouse Alexa Fluor 488, Donkey anti-rabbit Alexa
345 Fluor 555, and others were incubated for 1 hour at room temperature. DAPI (1:10000,
346 Molecular Probes) was used for nuclear staining. Based on images, cell orientation was
347 analyzed using the "OrientationJ" plugin in Fiji. Normalization was done to the sum of all
348 values. The orientation charts were created using Python's "Matplotlib" library to visualize data
349 in a polar coordinate system. The data, consisting of angles and corresponding values, was
350 loaded from a file based on the measurements from Fiji. To enhance visual clarity, a polar bar
351 plot was generated with customized colors, borders, and transparency. The plot's axis was
352 adjusted to display angles from -90° to 90°, with the zero-angle positioned at the top.
353 To estimate cell migration and distribution throughout the conduit, we performed fluorescent
354 cell labeling. Cells used for seeding at one end of the conduit were labeled with CellTrace™
355 Far Red DDAO-SE (C34564, Thermo Fisher), while cells seeded at the opposite end were

356 labeled with the CellTrace™ CFSE Cell Proliferation Kit (C34554, Thermo Fisher).
357 Specifically, F11 cells were stained with 10 μM of CellTrace™ Green CMFDA and
358 CellTracker™ Deep Red according to the manufacturer's protocol. Briefly, cells were
359 incubated with the fluorescent dyes (1:1000 dilution in DMEM) for 20 minutes at 37 °C,
360 followed by five washes with PBS. After staining, cells were centrifuged at 400 × g for 5
361 minutes, resuspended in 10 mL of complete medium, and centrifuged again. The labeled cells
362 were then used to prepare the collagen-mTG bioink, as described in section 2.11. Each stained
363 cell population was used to bioprint into opposite ends of the GrooveNeuroTube. Specifically,
364 500 μL of collagen-based bioink containing 250,000 labelled-cells was bioprinted onto one end
365 of the conduit as described in 2.11. The same procedure was repeated for the opposite end using
366 the second cell population. After 28 days of culture under standard and PEMF conditions,
367 constructs were fixed in 4% paraformaldehyde overnight at 4 °C. The next day, the samples
368 were washed three times (30 minutes each) in PBS on a rotary shaker, embedded in 6% agarose
369 (Condalab, 8017.00), and sectioned transversely into 300 μm slices using a vibratome (Leica
370 VT100S). The central sections were immersed in PBS and stained with DAPI (1:10,000;
371 Molecular Probes) for nuclear visualization. Fluorescence imaging was performed using a
372 confocal microscope (Olympus FV1200) with a 10× dry objective and excitation lasers at
373 405 nm, 488 nm, and 635 nm. Emission signals were collected in the ranges of 430–460 nm for
374 DAPI (excited at 405 nm), 510–520 nm for CFSE (excited at 488 nm), and 630–640 nm for
375 CellTrace™ Far Red (excited at 635 nm). A 10×/NA 1.2 dry objective was used for imaging.
376 After 28 days in culture, fluorescence imaging clearly showed co-localization of both labeled
377 cell populations in the central region of the conduit, confirming that cells seeded from opposite
378 ends successfully migrated and met in the middle. All experiments were performed with four
379 biological repeats and three experimental repeats.

380 **2.14. Cytotoxicity assessment**

381 For live/dead visualization, sections were incubated with 2 μM Calcein-AM and 2 μM
382 Ethidium homodimer-1 in PBS at 37°C for 30 minutes. The cells were visualized on confocal
383 laser scanning microscope (Zeiss LSM 780 NLO, Olympus FV1200) with a 40× water
384 objective and excitation laser wavelengths of 561 nm for EthD-1 and 488 nm for Calcein-AM
385 and emission of 500-520 nm and 600–630 nm, respectively. The live-to-dead cell ratio from
386 live/dead measurements was calculated by dividing the number of live cells by the total cell
387 count (sum of live and dead cells) and expressing it as a percentage for each time point. The
388 percentage of dead cells was obtained by subtracting the percentage of live cells from 100%.
389 Next, the increase in live cell growth was calculated relative to day 1 by normalizing the live
390 cell count at each subsequent time point to the initial value. The number of live cells on day 1
391 was set as 100%, and the percentage increase was calculated using the formula: Live Cell
392 Growth (%) = (Live Cells at given time point / Live Cells at day 1) × 100%. These calculations
393 were performed to assess cell viability and proliferation trends over time, including the effects
394 of PEMF stimulation. To perform a quantitative viability assay using flow cytometry (MUSE),
395 the commercial Muse™ Annexin V & Dead Cell Kit was used. For sample preparation, the
396 cell cultures after 14 days of incubation with respective materials were washed with PBS,
397 trypsinized, centrifuged, and resuspended in 100 μL of PBS with 1% FBS. Then, 100 μL of
398 the reagent was added, and the mixture was incubated for 20 minutes in the dark at room
399 temperature. Finally, the collected data were analysed using Flowing Software 2. Another
400 experiment conducted was the detection of reactive oxygen species (ROS) using the Muse®
401 Oxidative Stress Kit. Cells were collected from the culture in the same manner as for the
402 viability test. The positive control consisted of cells seeded the day before and treated with
403 menadione one hour prior to measurement. After the measurements, the results were analysed
404 using Flowing Software 2.

405 **2.15. Immunocytochemistry and quantification**

406 Cells cultured on all surfaces for 2, 7, 14, and 21 days were rinsed twice with PBS (phosphate-
407 buffered saline, Sigma-Aldrich) and incubated for 15 min with 2.5% formaldehyde solution in
408 PBS at T = 21 °C. Then, the cells were permeabilized by PBS containing 0.5% Triton X-100,
409 washed with PBS, blocked with 3% BSA in PBS, and incubated with primary antibodies for 1
410 hour at room temperature. The following primary antibodies were used to detect antigens:
411 rabbit anti-Dcx (IgG, 1:100, 48-1200, ThermoFisher), mouse anti-Map2 (IgG1, 1:250, 13-
412 1500, ThermoFisher), rabbit anti-Syp (IgG, 1:100, ab32127, Abcam). After washing with PBS,
413 the secondary antibodies were used to react with the cells for 1 hour at room temperature. The
414 following secondary antibodies were used: Donkey anti-mouse (Alexa Fluor 488, 1:200,
415 a24350, ThermoFisher), Goat anti-rabbit IgG (H+L) (Alexa Fluor 647, a32733,
416 ThermoFisher), Goat anti-mouse IgG (Alexa Fluor 488, a32723, ThermoFisher). Finally, cells
417 were stained by 4',6-diamidyno-2-fenyloindol (DAPI) and imaged immediately using Zeiss
418 LSM 780 NLO and Olympus FV1200 confocal microscope with 40× microscope water
419 objective. All measurements were repeated at least three times. The MAP2/SYP/DCX positive
420 cells were determined manually from at least 500 cells taken from random
421 immunocytochemical (ICC) staining. DRG cells were quantified by counting the number of
422 MAP2+ and/or SYP/DCX+ cells possessing a neuronal morphology expressed as a percentage
423 of DAPI-stained nuclei per condition.[36] Neurite outgrowth was characterized by measuring
424 the most extended neurite length for each MAP2/SYP positive cell. As reported previously, at
425 least 100 DCX/MAP2/SYP positive cells per sample were included in the measurement.[37]

426 **2.16. RNA isolation and RT-qPCR**

427 The series of real-time polymerase chain reaction (qPCR) experiments were conducted on F11
428 DRG neural cells using designed primers (***Table S1***). Obtained cell suspensions were used for
429 RNA isolation. RNA was isolated using the Aurum Total RNA Mini Kit (Bio-Rad), yielding
430 >500 ng/μL of RNA. During the isolation, DNase treatment was performed to eliminate any

431 remaining genomic DNA that could potentially amplify during PCR reactions. Subsequently,
432 reverse transcription reactions were performed using 1 µg of RNA and the iScript cDNA
433 Synthesis Kit (Bio-Rad) in a volume of 20 µL. The cDNA synthesis reaction conditions were
434 as follows: 5 min at 25°C, 20 min at 46°C, 1 min at 95°C. The obtained cDNA served as a
435 template for PCR reactions using gene-specific primers, including GAPDH, ACTB, DCX,
436 MAP2, TUBB3, SYP, SYN, s100b, and peripherin. The cDNA samples were diluted 2.5x and
437 reaction was carried out using 2 µL of cDNA template and Taq PCR Master Mix (Qiagen). The
438 exemplary PCR reaction conditions were as follows: initial denaturation at 94°C for 3 min,
439 denaturation at 94°C for 30 s, primer annealing at 60°C for 30 s, extension at 72°C for 60 s (35
440 cycles), and final extension at 72°C for 10 min. The PCR products were separated on a 1.5%
441 agarose gel, and by comparing them to a size marker (Puc19/msp1), specific products
442 corresponding to 104 bp for ACTB, 158 bp for GAPDH, 151 bp for MAP2, and 89 bp for
443 TUBB3 were confirmed. The PCR products for ACTB, GAPDH, MAP2, and TUBB3 were
444 excised from the gel and purified using the QIAquick Gel Extraction Kit (Qiagen). The
445 amounts of DNA obtained for each sample were quantified in ng/µL and are presented in
446 Supplementary materials. Subsequently, molecular quantities per µL were calculated based on
447 the product size and DNA concentration, and decimal dilutions were performed.

448 **2.17. Pulsed electromagnetic fields (PEMF) device and stimulation**

449 For the PEMF tests, we used an in-house stimulation system (***Figure S7***). The system could
450 generate sinusoidal, triangle, and square waveform functions in the 0.1 Hz - 10 MHz frequency
451 range. A smaller 50-500 Hz range was used as a sinusoidal wave for cell stimulation.
452 Synthesized Function Generator SFG-2000/SFG-2100 Series (GW INSTEK) was used to
453 generate alternating current: sinusoidal, triangle, and square-shaped of various frequencies.
454 The shape of the curves was confirmed on the MDO-2000E series, which is a multi-functional
455 mixed-domain oscilloscope (GW INSTEK). Curer fed the six ferrite core coils (Viston art. no.

456 3808) under the 6-well polystyrene transparent multiwall plate. The magnetic field obtained
457 was measured on the bottom of the wells, and a magnetic field meter (TENMARS TM-197)
458 was used for AC magnetic measurements. The sterile closed cell culture in Petri dishes was
459 placed directly above the coils, providing a magnetic field. For the PEMF, we chose a
460 sinusoidal function of frequency 50 and 500 Hz, which generated magnetic field induction of
461 0.24 mT at the bottom of the well. The device was used to stimulate cells 4 h daily in the
462 incubator for the whole duration of the experiment.

463 **2.18. Antibacterial tests**

464 The optical density measurements at 600 nm (OD600) were carried out to monitor the growth
465 of microbes, i.e. *E.coli* and *S.aureus* in a liquid culture. The overnight cultures of 150 colony-
466 forming units (CFU)/mL *S.aureus* (150 μL) or *E.coli* (150 μL) were added to the tubes
467 containing 30 mL of fresh Luria broth (LB) medium. Discs of crosslinked HAMA1%-
468 GelMA8% containing lysozyme (0.5 mg/mL) (5 mm x 5 mm) were incubated for 1, 7, 14 and
469 21 days. Bacterial strains *E. coli* ATCC 35218 and *S. aureus* ATCC 29213 were grown in LB
470 Broth Lennox under continuous shaking at 250 rpm, at 37 °C, for 24 hours. Following
471 incubation, the bacterial cultures were diluted to achieve a final $5 \times 10^5$ cells/mL concentration
472 in LB broth. A volume of 100 μL of the prepared bacterial suspension was transferred into each
473 well of a 96-well plate. Fresh solutions of lysozyme at concentrations of 0.25, 0.5, 1, and 1.5
474 mg/mL were prepared and incubated for 1, 7, 14, and 21 days to simulate conditions resembling
475 those found in hydrogels stored/incubated in the incubator. These pre-incubated lysozyme
476 solutions were introduced into the wells alongside the bacterial cultures and incubated at 37 °C
477 for 24 hours. The bacterial growth was assessed by measuring the optical density (OD600)
478 using an Infinite M200 Pro microplate reader (Tecan) after incubation. To minimize any
479 potential interference caused by the light-scattering properties of the samples, control wells
480 containing the same concentrations of lysozyme in LB broth but without bacteria were included

481 as blank controls. For comparison, untreated bacterial cultures served as the negative control,
482 while bacterial cells exposed to antibiotics were used as the positive control. All experiments
483 were conducted in triplicate to ensure reproducibility and reliability of the data.

484 Subsequently, a 0.5 mg/mL lysozyme concentration was selected for further studies.
485 The HAMA-GelMA hydrogel containing 0.5 mg/mL lysozyme was prepared as described in
486 the previous sections. The hydrogel, immersed in PBS, was placed in an incubator for the
487 duration of the experiment. After 7, 14, and 21 days of incubation, 100 μL of the PBS
488 supernatant was collected, and bacteria at the same concentration as in the previous experiment
489 were added to the PBS supernatant containing lysozyme released from the HAMA-GelMA
490 hydrogel. A volume of 100 μL of the prepared bacterial suspension mixed with the lysozyme-
491 containing PBS supernatant was transferred into each well of a 96-well plate. Optical density
492 (OD600) measurements were taken after 24 hours, following the same procedure as in the
493 previous experiment.

## 3. Results and Discussion

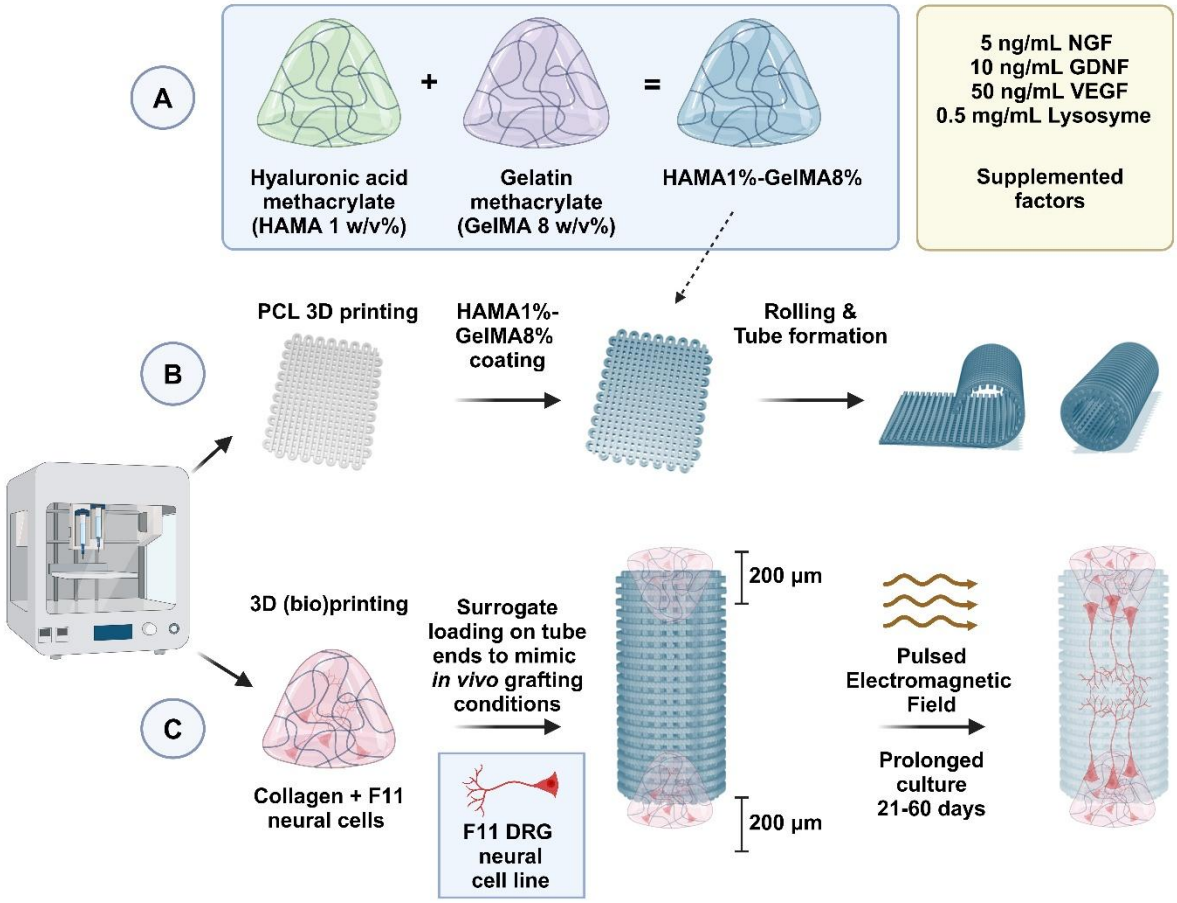


***Figure 1***: *A) Preparation of the hydrogel formulation: Hyaluronic acid methacrylate (HAMA, 1 w/v%) is combined with gelatin methacrylate (GelMA, 8 w/v%) to produce the composite hydrogel, referred to as HAMA1%-GelMA8%. Selection of supplemented growth factors and antimicrobial lysozyme is noted in a separate table. B) Fabrication of the scaffold tube: A polycaprolactone (PCL) grid is first 3D-printed, followed by coating with the HAMA1%-GelMA8% hydrogel. Subsequently, the coated grid is rolled and formed into a tubular structure. C) 3D (Bio)printing and stimulation: Collagen mixed with F11 DRG neural cells are bioprinted at both ends of the tubular construct to mimic in vivo grafting conditions, spanning roughly 200 µm injection side into the tube. The structure can then be subjected to pulsed electromagnetic field (PEMF) stimulation and cultured for a prolonged period (21–60 days) to promote neural tissue outgrowth and integration. Created with BioRender.com.*

507 Peripheral nerve injuries are challenging to treat due to the slow regeneration rate and
508 limited functional recovery. Current NGCs often fail to replicate the biomimetic
509 microenvironment required for effective nerve repair. In this study, we developed a tubular
510 nerve conduit using a combination of 3D printing (***Figure 1B***) and bioengineered bioactive
511 hydrogel (***Figure 1A-C***) as a new *ex-vivo* model. Firstly, we formulated a composite hydrogel
512 consisting of hyaluronic acid methacrylate (HAMA, 1 w/v%) and gelatin methacrylate
513 (GelMA, 8 w/v%), denoted as HAMA1%-GelMA8% (***Figure 1A***). A 3D-printed
514 polycaprolactone (PCL) grid scaffold was coated with this hydrogel, rolled into a tubular
515 structure, and used as a nerve conduit (***Figure 1B***). In a final step, cell-laden collagen was bio-
516 printed onto both ends of the tube to mimic *in vivo* grafting conditions. Subsequently, to
517 enhance neural regeneration, the conduit was subjected to a PEMF stimulation during
518 prolonged culture periods (21–60 days) (***Figure 1.C***). The hypothesis was to test our developed
519 *ex vivo*-like system and check if PEMF stimulation supported neural cell migration, alignment,
520 and outgrowth, mimicking the *in vivo* conditions.

521 **3.1 Fabrication of PCL fibers grid**

522 In this study, following previous reports on PCL groove-patterned surface topography and
523 its impact on neural cell differentiation and maturation [7, 38] we expand on this by exploring
524 the influence of PCL fibers and the stiffness of HAMA-GelMA hydrogel on the growth and
525 migration of neural DRG cells.

526 In the first part, we focussed on PCL fibers grid optimization. For this, we used various
527 printing temperatures (90 °C to 220 °C), different pressures (175–550 kPa), and printing speeds
528 (10–15 mm/s) to achieve consistent fibers with homogenous and reproducible layer-by-layer
529 grid structure. After the preliminary elimination of challenges (***Figure S1***), we selected the
530 following parameters for further studies: 90 °C, 180 kPa, and two printing speeds: 10 mm/s
531 (abbreviated as 10N) and 15 mm/s (abbreviated as 15N). Both selected printing speeds enabled

532 the generation of reproducible fibers (***Figure 2A***). For samples printed at 10 mm/s, the average
533 fiber diameter was 96.1 ± 18.3 µm. At 15 mm/s, the average fiber diameter was 79.5 ± 19.7
534 µm (***Figure 2 A, E***), where the square size between all fibrillar constructs defines porosity.
535 After printing two layers of PCL fiber grids, the structure was rolled into a tube (***Figure 2B,***
536 ***D***). The PCL fibers were tightly rolled three times to form a tube measuring 16.5 mm long and
537 7.4 mm in diameter. To secure the structure and prevent it from unrolling, a section of the sheet
538 was bonded to the tube by applying additional PCL fibers using the thermoplastic printhead of
539 the BioX2, heated to 60°C (***Figure 2 B, D***). We then investigated the topography of the
540 produced PCL fibers and grids using optical microscopy and scanning electron microscopy
541 (SEM). We confirmed it formed a regular structure (***Figure 2 A-D***).
542
543
544

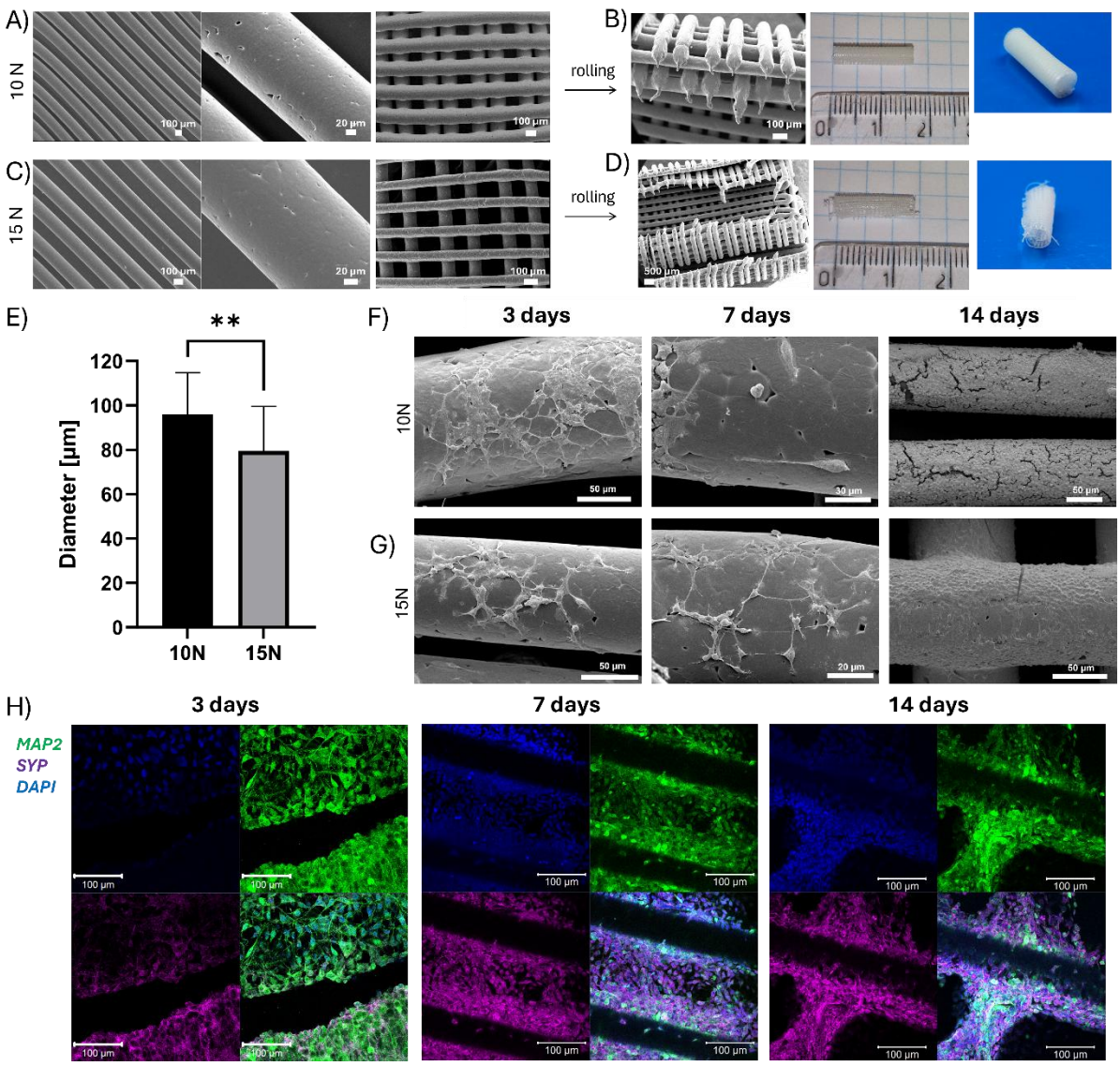


***Figure 2:*** *Optimization of 3D printing of PCL fibers: A) 10N and C) 15N, B, D) SEM morphological characterization of 3D printed PCL grid which we used to form multilayer tube. E) diameter of PCL fibers, F, G) SEM images of F11 DRG neural cells cultured on a PCL grid for 3,7, and 14 days. H) Confocal images of F11 DRG neural cells cultured on PCL showing the detection of late neuronal (green, MAP2) and synaptic vesicles (violet, SYP) markers.*

Subsequently, we cultured the F11 DRG neural cell line on the fabricated PCL grids for 3, 7, and 14 days and assessed their morphology using SEM (***Figure 2F, G***). On day 3, we observed that F11 cells cultured on larger N10 fibers exhibited a noticeably higher cell density

than smaller N15 fibers, likely due to the increased surface area of the N10 fibers. By day 7, F11 cells displayed a polarized, elongated morphology, indicating their alignment and adaptation to the scaffold structure. By day 14, the cells had formed extensive neurites and a dense cellular network on both types of fibers, with a visibly more robust network observed on the N10 grid, further emphasizing the advantages of the larger fiber diameter for neural cell growth and improved cell-cell connectivity (***Figure 2F, G***). From the two choices, the 10N PCL grid proved to be more stable, easier to roll and retained more coherent smooth structure (***Figure 2A-D***). It also appeared to provide better F11 DRG neural cells maturation (***Figure 2F***). Therefore, for all the subsequent evaluations we selected 10N PCL grids and tubes.

To confirm the functional process of neuronal maturation, we performed immunocytochemistry (ICC) to detect MAP2 (Microtubule-Associated Protein 2), a marker of mature neurons, and SYP (Synaptophysin), a protein characteristic of synaptic vesicles and considered a synaptic marker. MAP2+/SYP+ cells were identified across both grid types ***(Figure 2H***). With extended culture duration, the number of SYP+ cells increased, indicating enhanced synaptic activity, while MAP2+ levels remained relatively constant. The most prominently elongated MAP2+/SYP+ cells were observed on day 14, often in close contact with the neighbouring cells. This observation suggests the potential formation of neural-like networks, indicating ongoing neuronal maturation (***Figure 2H***).

**3.2 Development of HAMA-GelMA composite hydrogel**

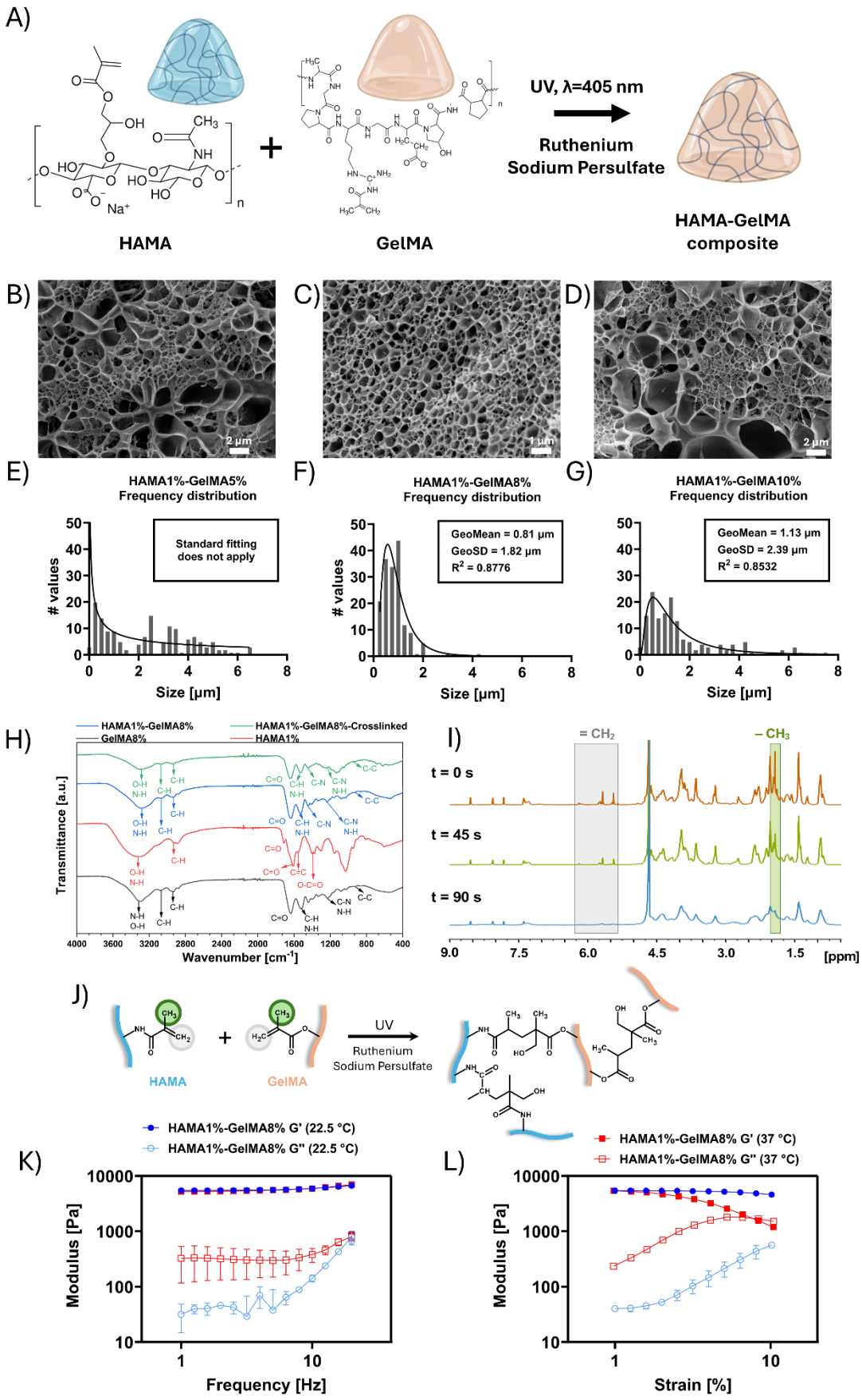
A)
HAMA
GelMA
UV, λ=405 nm
Ruthenium
Sodium Persulfate
HAMA-GelMA
composite
B)
C)
D)
E)
HAMA1%-GelMA5%
Frequency distribution
Standard fitting
does not apply
F)
HAMA1%-GelMA8%
Frequency distribution
GeoMean = 0.81 µm
GeoSD = 1.82 µm
R² = 0.8776
G)
HAMA1%-GelMA10%
Frequency distribution
GeoMean = 1.13 µm
GeoSD = 2.39 µm
R² = 0.8532
# values
Size [µm]
H)
HAMA1%-GelMA8%
HAMA1%-GelMA8%-Crosslinked
GelMA8%
HAMA1%
Transmittance [a.u.]
Wavenumber [cm⁻¹]
I)
= CH₂
– CH₃
t = 0 s
t = 45 s
t = 90 s
[ppm]
J)
HAMA
GelMA
UV
Ruthenium
Sodium Persulfate
K)
HAMA1%-GelMA8% G' (22.5 °C)
HAMA1%-GelMA8% G'' (22.5 °C)
Modulus [Pa]
Frequency [Hz]
L)
HAMA1%-GelMA8% G' (37 °C)
HAMA1%-GelMA8% G'' (37 °C)
Modulus [Pa]
Strain [%]

581 ***Figure 3:*** *A) Scheme of HAMA-GelMA composite formation. CryoSEM of B) HAMA1%-*
582 *GelMA 5% C) HAMA1%-GelMA 8% D) HAMA1%-GelMA10% E,F,G) pore size frequency*
583 *distribution of each associated formulation H) FTIR spectra of HAMA, GelMA, and HAMA1%-*
584 *GelMA8% composite hydrogels; I)* $^{1}H$ *NMR spectra of non-crosslinked and crosslinked*
585 *HAMA1%, GelMA8%, and HAMA1%-GelMA8% at different time points (note reduced content*
586 *of crosslinker and initiator in methods to enable monitoring of the reaction); J) Schematic*
587 *representation of the photoinitiated crosslinking reaction between HAMA and GelMA under*
588 *UV irradiation in the presence of a redox initiator system; K) Amplitude sweep and L)*
589 *frequency sweep of the HAMA1%-GelMA8% composite*
590
591 Next, we evaluated the selection of composite hydrogels made from HAMA and
592 GelMA. In similar composite formation, HAMA concentration was fixed at 1%, whereas
593 secondary polymer concentration modulated to obtain desired properties, which we decided to
594 follow through.[39] ***Figure 3A*** presents a schematic illustration of the composite hydrogel
595 formation, showing the chemical composition of the two chosen polymers, HAMA and
596 GelMA. In the first instance, we performed Cryo-SEM imaging of HAMA1%-GelMAX%
597 hydrogels, where X indicates variable content of GelMA, going from 5, 8 to 10% (***Figure 3B-***
598 ***D***). All micrographs demonstrated interconnected porous structures of hydrogels. HAMA1%-
599 GelMA8% displayed the most homogenous structure across all tested hydrogels, with the
600 average porosity obtained from lognormal distributed in the 0.81 ± 1.82 μm range (***Figure 3E-***
601 ***G***). This was much smaller than for the HAMA1%-GelMA5%, for which a non-standard
602 broader distribution that could not fit with any standard model was obtained.
603 The FTIR spectra of GelMA8% in (***Figure 3-H***) show several characteristic peaks. The
604 broad peak 3300 $cm^{-1}$ represents the stretching vibrations of O-H and N-H groups. Peaks within
605 the range of 3100–2800 $cm^{-1}$ are attributed to C-H stretching vibrations. The signature amide

606 bonds of gelatin are evident at 1630 $cm^{-1}$, corresponding to C=O stretching of amide I, 1520
607 $cm^{-1}$ attributed to N-H bending coupled with C-H stretching of amide II, 1226 $cm^{-1}$ signifies
608 the C-N stretching and N-H bending of amide III, and 926 $cm^{-1}$ indicating -C-C- skeletal stretch
609 of amide IV.[40, 41]

610 In HAMA1% spectra broad peak around 3300 $cm^{-1}$ indicate the stretching vibrations of
611 O-H and N-H, while the peak at 2900 $cm^{-1}$ represents C-H stretching. The region between 1710
612 $cm^{-1}$ and 1450 $cm^{-1}$ shows overlapping of amide I and amide II peaks along with C=O bending
613 vibrations.[42-44] Peaks at 1553 $cm^{-1}$ and 1290 $cm^{-1}$ indicate stretching vibrations of C=C and
614 O-C of methacrylate.[45] Additionally, the peak at 1410 $cm^{-1}$ corresponds to stretching
615 vibrations of O-C=O groups.[46]

616 In the composite HAMA1%-GelMA8% hydrogel, the dominant peaks of GelMA due
617 to its higher concertation are observed along with the characteristic feature of both the
618 components at 1150 $cm^{-1}$ represents the C-O bending stretching, respectively.[46] In the
619 crosslinked HAMA1%-GelMA8% hydrogel, the characteristic peaks of gelatin and hyaluronic
620 acid remain intact. However, the peak of C=C stretching of methacrylate group is too close to
621 the amide I region of gelatin, making it difficult to decouple the signals for any analysis.[47]
622 Slight variations in the intensities and position of the peaks 1500–1000 $cm^{-1}$ suggests chemical
623 interactions or physical blending between the HAMA1% and GelMA8% components. The
624 described changes in the composite spectrum indicate that HAMA1% and GelMA8% interact
625 well to form a composite hydrogel with small alterations to the chemical bonding and
626 molecular structure compared to the individual components.

627 To confirm the photo-crosslinking of HAMA1%-GelMA8% hydrogels $^{1}H$ NMR
628 analysis was performed as shown in ***(Figure 3-I)***. The spectra were recorded at different UV
629 irradiation times, allowing for the observation of changes as the exposure progressed. The
630 process was evidenced by the gradual disappearance of the signals corresponding to the protons

631 of methacryloyl vinyl (~5.6 – 6.2 ppm) and methyl groups (~1.9 ppm). Initially, at t = 0 s,
632 these resonances were clearly visible, indicating the presence of unreacted methacryloyl
633 moieties, similarly to the published GelMA and HAMA systems.[32, 39] After 45 s of UV
634 exposure, their intensities decrease, and by 90 s, they are nearly absent. This indicates that the
635 methacryloyl vinyl groups underwent a reaction initiated by radicals formed during
636 photoinitiation, leading to their 'consumption' as they participated in the formation of new
637 covalent bonds. The disappearance of the vinyl and methyl proton resonances confirms the
638 ongoing reaction between the polymer chains. Furthermore, the broadening of the resonances
639 observed in the last spectrum can be attributed to an increase in the heterogeneity of the
640 chemical environment of the protons and the restriction of polymer chain mobility within the
641 forming crosslinked network. The increased structural rigidity of the created three-dimensional
642 network leads to shortening $T_2$ relaxation times, contributing to peak broadening. These
643 observations provide clear evidence of methacrylate depletion, indicating that the primary
644 cross-linking mechanism is a radical-mediated reaction between the vinyl moieties of
645 methacryloyl groups, leading to the formation of a crosslinked composite and corroborating
646 with the FTIR results. The vinyl groups of the methacryloyl moieties undergo radical
647 polymerization, forming covalent crosslinks between polymer chains (***Figure 3I, J***).

648 For a selected HAMA1%-GelMA8% formulation, we run both amplitude (***Figure 3K***)
649 and frequency sweeps (***Figure 3L***) to establish their rheological properties (after crosslinking),
650 both at room temperature (set as 22.5 °C) and at physiological temperature (37°C). Amplitude
651 sweep demonstrated that cross-linked hydrogels largely retained their viscoelastic nature at the
652 higher temperature, with similar storage modulus at 1% strain (***Figure 3J***). The linear
653 viscoelastic region (LVR) was noted to be much shorter at the 37 °C, indicating the underlying
654 gelatine chains pertain slight temperature responsiveness. Nevertheless, storage modulus still
655 dominated over loss modulus, indicating a soft hydrogel-like structure was persistent.

Frequency sweep revealed no difference between the composite HAMA1%-GelMA8% the two tested at two different temperatures (5480 ± 30 Pa at 22.5 °C and 5200 ± 290 Pa at 37 °C), taken at 1 Hz.

### 3.3. Investigation of F11 DRG Neural Cells 2D Behaviour on HAMA-GelMA Hydrogels

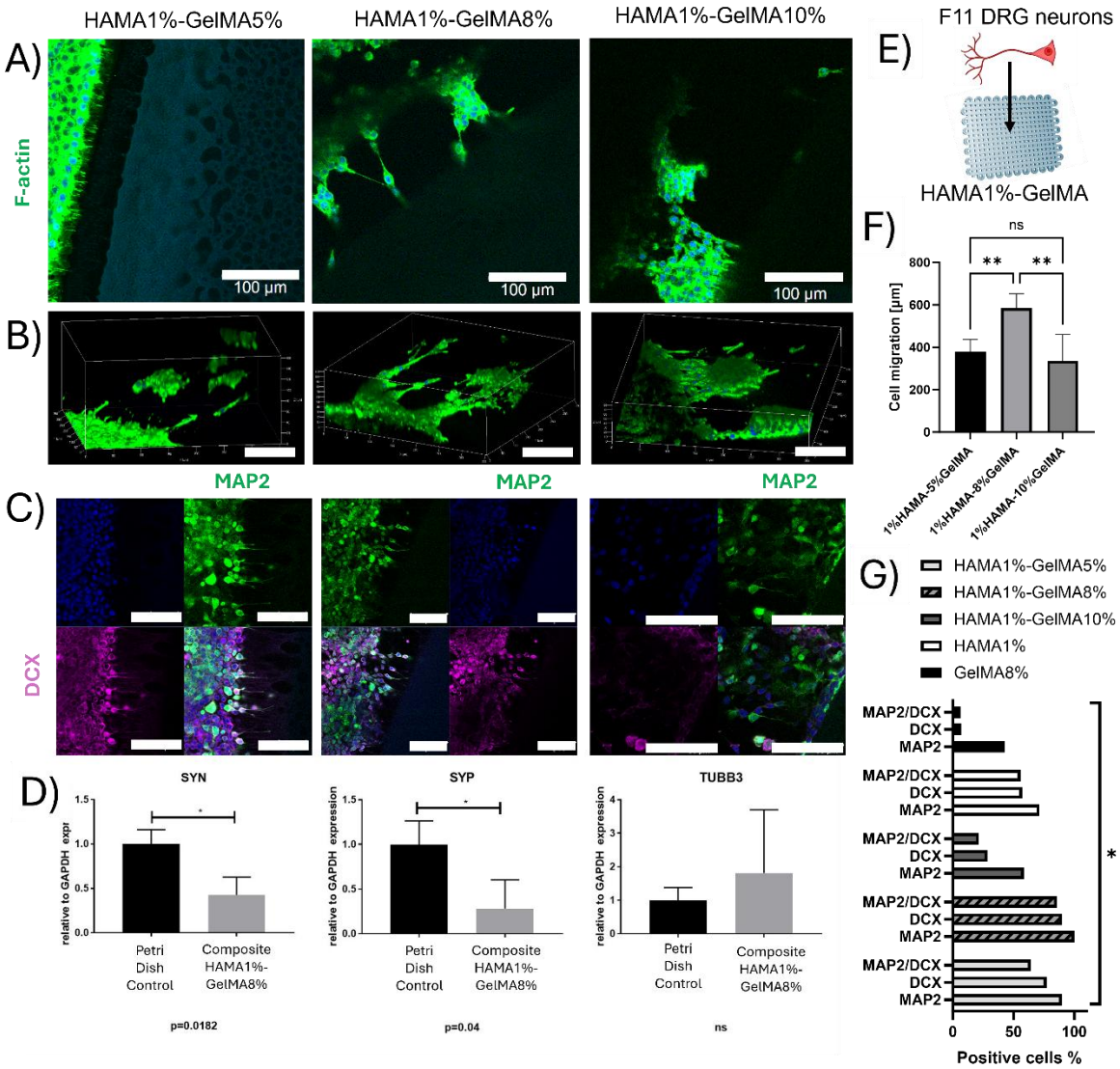


***Figure 4:*** *Immunocytochemical images from confocal microscopy showing F11 DRG neural cells cultured on the top of composite for 7 days A) HAMA1%-GelMA5%, HAMA1%-GelMA8%, HAMA1%-GelMA10%, stained to visualize F-actin; B) 3D reconstruction of Z-stacks; C) ICC detection of migrating (DCX, violet) and late (MAP2, green) neuronal markers in cells cultured on HAMA-GelMA composite hydrogels for 14 days. The scale bar represents 100 µm in all images. D) The differences in relative expression of the SYN, SYP and TUBB3*

667 *genes (relative to GAPDH) for F11 DRG neural cell line cultured on a top of composite*
668 *hydrogel for 7 days. Control indicates cells cultured in standard Petri Dish. Statistical analysis*
669 *was performed using student t-test (performed in GraphPad software) with three biological*
670 *replicates. Data are presented as mean ± standard deviation; *p<0.05.*
671
672 In this step, we investigated F11 DRG neural cell growth on the 2D surface of 500 µL
673 hydrogel layers and analysed cell migration, morphology, viability, and the expression of
674 neural markers. Three composite hydrogel types with varying GelMA concentrations (5%, 8%,
675 and 10%) were tested, while the HAMA concentration remained constant at 1%. After 7 days
676 of culture, the samples were fixed and stained for F-actin to visualize the cytoskeleton. Cell
677 migration at HAMA1%-GelMA8% was 53.68% higher than at HAMA1%-GelMA5% and
678 73.81% higher than at HAMA1%-GelMA10%. The greatest, statistically significant cell
679 migration was observed for the HAMA1%-GelMA8% hydrogels, compared to GelMA5% and
680 GelMA10%, and therefore, they were subsequently selected for further studies (***Figure 4A, B,***
681 ***F***).
682 To assess the migration and maturation of DRG neural cells, immunodetection of proteins
683 associated with migrating (doublecortin, DCX) and late (Microtubule Associated Protein 2,
684 MAP2) neuronal markers was performed after 14 days of culture ***(Figure 4C***). The results
685 demonstrated DCX/MAP2+ cells across all tested samples, but the most favourable cell
686 morphology was observed on the HAMA1%-GelMA8% and HAMA1%-GelMA5%. Cell
687 migration was not significant for the HAMA1%-GelMA5% samples, while the HAMA1%-
688 GelMA10% hydrogels exhibited fewer DCX/MAP2+ cells in the observed sections. The results
689 show that the composite hydrogel HAMA1%-GelMA8% demonstrated the highest percentage
690 of MAP2/DCX positive cells, pointing towards its most effective support for neural cell
691 migration. Specifically, 90% of cells were DCX+, while 85% were both MAP2/DCX+ (***Figure***

692 ***4G***). In comparison, HAMA 1%-GelMA5% exhibited 77%, and HAMA1%-GelMA10%, 28%,
693 significantly lower effectiveness. Interestingly, the individual control hydrogels, HAMA1%
694 and GelMA8%, did not support DCX expression as effectively, yielding only 57% DCX+ cells
695 for HAMA, and a mere 7% DCX+ cells for GelMA8% (***Figure S2A, B***). Cells cultured on 1%
696 HAMA or 8% GelMA also did not exhibit proper elongated morphology and contained very
697 few DCX/MAP2+ cells after two weeks of culture (***Figure S2A-B*** and ***Figure 4G***). These
698 findings suggest that the HAMA1%-GelMA8% hydrogel composition is optimal for promoting
699 the migration of F11 DRG neural cells and supporting the presence of both MAP2+ mature
700 neurons and DCX+ migrating cells, making it the most promising candidate for further
701 investigation (***Figure 4A, B, F***).Following systematic optimization, 8% GelMA was selected
702 as the optimal base concentration that provided a balance between mechanical support and
703 biological permissiveness, enabling efficient neural cell migration. Using this fixed GelMA
704 concentration, we further investigated the effect of varying HAMA content (0.5%, 1%, 2%,
705 and 5%) on neural cell migration, neurite outgrowth, and neural marker expression. We
706 observed the HAMA 1%–GelMA 8% hydrogel formulation was the most favorable for
707 promoting both neural cell migration and neurite elongation (***Figure S3A***). When using lower
708 HAMA concentrations, such as 0.5%, we did not observe neurite outgrowth, due to insufficient
709 mechanical integrity of the hydrogel matrix, which may degrade too rapidly or lack adequate
710 structural support for directed neurite extension. Conversely, at higher HAMA concentrations
711 (≥2% in combination with 8% GelMA), we observed reduced cell migration and limited neurite
712 elongation, potentially due to increased matrix stiffness and decreased porosity, which may
713 hinder cellular mobility and diffusion of signaling molecules. These findings are consistent
714 with the literature, which highlights that the relationship between hyaluronic acid (HA)
715 concentration and neural cell behavior is non-linear. Studies have shown that there is an optimal
716 HA concentration range that supports maximal neurite outgrowth and cell motility. For

717 example, hydrogels that are too stiff (e.g., at higher HA concentrations) can impede neurite
718 extension due to mechanical constraints, whereas hydrogels that are too soft (e.g., at 0.5%) may
719 degrade prematurely or lack structural cues needed for stable neurite anchorage [3, 12, 19].
720 Therefore, the HAMA 1%–GelMA 8% formulation appears to offer a balanced mechanical and
721 biochemical environment that facilitates both migration and neurite elongation. To further
722 analyse the expression of genes characteristic of neural cells, real-time qPCR was performed
723 using primers for the markers SYP, SYN, and TUBB3. The expression of synaptic markers
724 SYN and SYP significantly decreased in cells cultured on the composite hydrogels ($p<0.05$).
725 In contrast, the expression of the TUBB3 gene, associated with neuronal cytoskeleton
726 formation, only appeared to increase (not significant) compared to the two single component
727 hydrogels (***Figure S2A, B***). We also performed immunocytochemical staining after 7 days in
728 culture to detect markers of differentiated neurons, Tubulin Beta-III (TUBB3), and
729 Synaptophysin (SYP), also known as the significant synaptic vesicle protein p38. These
730 markers were identified in all materials we tested; however, we observed the highest number
731 of TUBB/SYP positive cells, especially for composite hydrogel (***Figure S2C, D, E, F***). The
732 expression of the TUBB3 gene was upregulated (not significant) at HAMA1% and HAMA-
733 GelMA8% compared to the flat control Petri dish (***Figure S2 G***).

734 To further evaluate cell viability, fluorescence imaging was conducted using Calcein-
735 AM (green) and ethidium homodimer-1 (red) after 1 and 5 days of incubation. Only live cells
736 with proper morphology were observed, and no dead cells were detected, confirming the
737 biocompatibility of the HAMA1%-GelMA8% hydrogel (***Figure S3***). Cell viability was
738 assessed using flow cytometry with the Muse™ Annexin V & Dead Cell Kit. Control cells
739 showed 98.3% survival. The results show that the cell viability of all tested materials is similar
740 to that observed for cells cultured on the HAMA-GelMA hydrogel, suggesting that the material
741 is not cytotoxic to F11 DRG neural cells. The comparison of cell viability across different

742 substrates indicates that the tested material does not cause a significant decrease in live cell
743 numbers, confirming its biocompatibility (***Figure S4***). Reactive oxygen species (ROS) were
744 detected using the Muse® Oxidative Stress Kit. The positive control, treated with menadione,
745 showed a significant increase in ROS-positive (ROS+) cells (approximately 60%). The lowest
746 ROS levels were observed in cells cultured on HAMA1%, while PCL and HAMA1%-
747 GelMA8% embedded in PCL grid (***GrooveNeuroTube***) substrates showed minimal
748 differences. The highest ROS levels were induced in cells cultured on GelMA8% hydrogels,
749 which confirms that the selected conditions for HAMA and the method of hydrogel preparation
750 positively influence cell viability and do not lead to ROS generation (***Figure S5***). The elevated
751 ROS in GelMA 8% is likely attributed to the high concentration of methacrylated gelatin and
752 the associated photo-crosslinking process. UV-induced polymerization in the presence of
753 photoinitiator can generate free radicals and residual oxidative species that persist in the
754 hydrogel network and stimulate intracellular ROS production. Moreover, the high density and
755 stiffness of 8% GelMA may limit oxygen and nutrient diffusion, further exacerbating cellular
756 oxidative stress. The GrooveNeuroTube scaffold, incorporating this hydrogel into a PCL
757 conduit, further decreased ROS to ~20%, approaching levels observed for HAMA 1% alone.
758 This progressive reduction indicates that combining GelMA with HAMA and structuring the
759 composite within a 3D scaffold effectively mitigates oxidative stress in neural cells.
760
761
762

763 **3.4. Impact of growth factors on cell behavior**

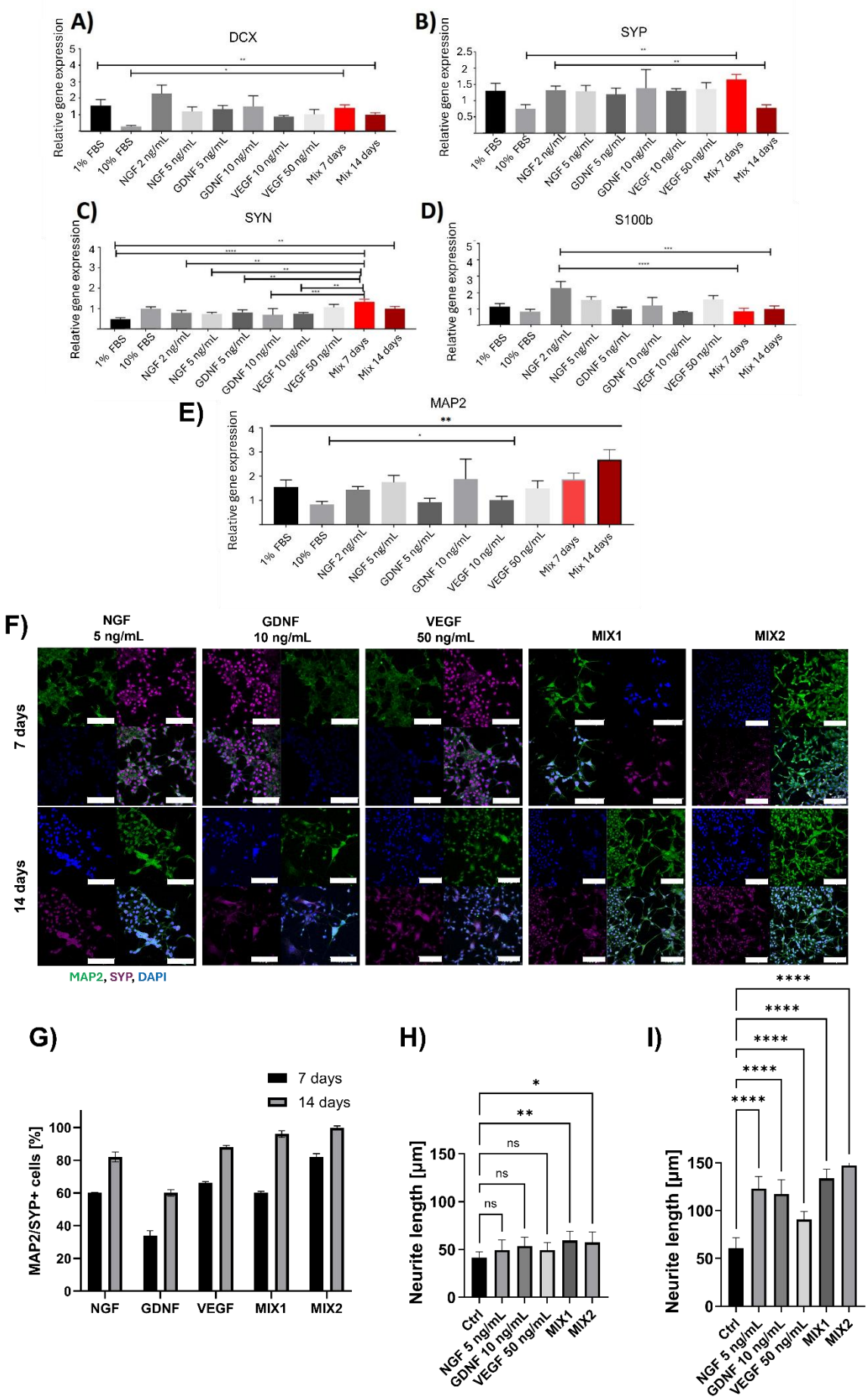
A)
DCX
B)
SYP
C)
SYN
D)
S100b
E)
MAP2
Relative gene expression
1% FBS
10% FBS
NGF 2 ng/mL
NGF 5 ng/mL
GDNF 5 ng/mL
GDNF 10 ng/mL
VEGF 10 ng/mL
VEGF 50 ng/mL
Mix 7 days
Mix 14 days
F)
NGF 5 ng/mL
GDNF 10 ng/mL
VEGF 50 ng/mL
MIX1
MIX2
7 days
14 days
MAP2, SYP, DAPI
G)
7 days
14 days
MAP2/SYP+ cells [%]
NGF
GDNF
VEGF
MIX1
MIX2
H)
Neurite length [µm]
ns
Ctrl
NGF 5 ng/mL
GDNF 10 ng/mL
VEGF 50 ng/mL
MIX1
MIX2
I)
Neurite length [µm]
Ctrl
NGF 5 ng/mL
GDNF 10 ng/mL
VEGF 50 ng/mL
MIX1
MIX2

764

765 ***Figure 5:*** *The differences in the relative expression of the A) DCX, B) SYP, C) SYN, D) S100b,*
766 *and E) MAP2 genes (relative to GAPDH) for F11 DRG neural cell line cultured in the presence*
767 *of growth factors for 7 and 14 days. F) Visualization of F11 DRG neural cells subjected to*
768 *growth factors for 7 and 14 days. Representative confocal images immunostained for MAP2*
769 *(mature neurons; green) and SYP (synaptic marker, violet) (bottom panel) cultured for 21 days*
770 *in the presence of different growth factors and their mixes. The scale bar represents 100 µm in*
771 *all images. G) The histograms show the quantification of positive to total number of cells*
772 *corresponding to MAP2/SYP+. Neurite length after culture of H) 7 days and I) 14 days with*
773 *GFs. Statistical analysis was performed using One-Way ANOVA (performed in GraphPad*
774 *software) with Tukey's post hoc test. Data are presented as mean ± standard deviation; n=3,*
775 **p<0.05, **p<0.01, ***p<0.001, ****p<0.0001.*

776 In the next phase, we aimed to demonstrate the functionality of the hydrogels as a matrix
777 that can further deliver a cocktail (mix) of selected growth factors. For this, we first selected
778 several growth factors and chose their concentrations based on literature data[48-50]: NGF 2
779 ng/mL and 5 ng/mL, GDNF 5 ng/mL and 10 ng/mL, as well as VEGF 10 ng/mL and 50 ng/mL.
780 In the first instance, to evaluate the general effects of growth factors on cells, we performed a
781 simple 2D culture of F11 DRG neural cells for 7 days with the addition of these. Results
782 revealed that the expression of neural-specific genes varied depending on the growth factor
783 applied (***Figure S6 A-D***). As FBS is known to affect biological responses, we wanted to
784 additionally tests its effects by modulating the concentration in the differentiating medium. In
785 particular, the analysis showed that DCX expression was significantly different between cells
786 cultured in 1% FBS (differentiating medium) and those in 10% FBS (standard culture medium).
787 The treatment of 2 ng/mL NGF notably increased DCX expression in the cells, while 5 ng/mL
788 NGF had an inhibitory effect (***Figure S6A***). The use of the other GF (GDNF, VEGF) resulted
789 in higher DCX expression compared to standard culture conditions (***Figure 5A***). The increase

790 in peripherin expression was observed with NGF at 2 ng/mL, GDNF at 10 ng/mL, and VEGF
791 at 50 ng/mL (***Figure S6B***). Treatment with 2 ng/mL NGF and 50 ng/mL VEGF stimulated
792 peripherin expression relative to 1% FBS culture (without statistical significance) and standard
793 culture with 10% FBS (statistically significant differences) (***Figure S6B***). For SYN and S100b,
794 increased expression was observed in samples treated with NGF and 50 ng/mL VEGF and 2
795 ng/mL, respectively (***Figure S6C, D***). Subsequently, to assess morphological changes, imaging
796 of cells cultured for 7 and 14 days was captured (***Figure 6F***). In those experiments, we tested
797 NGF (2 ng/mL and 10 ng/mL), GDNF (5 ng/mL and 10 ng/mL), and VEGF (10 ng/mL and 50
798 ng/mL). Given the noted individual effects of growth factors, we generated two selections of
799 their mixtures: **MIX1** contained 2 ng/mL NGF, 5 ng/mL GDNF, and 10 ng/mL VEGF, while
800 **MIX2** contained 10 ng/mL NGF, 10 ng/mL GDNF, and 50 ng/mL VEGF. After 7 days of
801 incubation, cells were collected by trypsinization, and proliferation and viability were assessed
802 using Trypan Blue staining. Results are summarized in ***Figure S6F-H.*** The results demonstrate
803 that cell numbers remained consistently high across all conditions over the 72-hour culture
804 period. Notably, the highest proliferation rates were observed in samples treated with **MIX1**,
805 reaching up to 3.3 million cells, suggesting that this combination provided the most favourable
806 environment for cell growth. Additionally, treatments with GDNF 10 ng/mL, VEGF 50 ng/mL,
807 and **MIX2** also promoted significantly higher cell numbers than the control, which maintained
808 a stable, albeit a lower count throughout the experiment. Importantly, prolonged culture did
809 not result in a decline in cell numbers, indicating that the experimental conditions effectively
810 supported sustained cell viability and proliferation (***Fig S6 F, G, H***).
811 F11 DRG neural cells displayed noticeable differences in morphology. The most prominent
812 observation was the elongation of neurites in cells treated with MIX1 and MIX2. Images of
813 F11 DRG neural cell morphology were captured after 7 and 14 days of culture using an optical
814 microscope (***Figure S6E***). It was noted that the growth factors influenced significant

815 differences in cell morphology. Elongated morphology and long neurites were observed in both
816 MIX-treated groups, suggesting the progression of neural maturation (***Figure S6E***).
817 The expression of the DCX gene in the samples after 14 days of culture significantly
818 increased in the 7-day culture compared to the 10% FBS control group but decreased in the 14-
819 day culture when compared to the 1% FBS group (***Figure 5A***). For the SYP gene expression,
820 a significant statistical increase was observed in the 7-day culture with the growth factor mix
821 compared to the 10% FBS control group, while a significant decrease was noted in the 14-day
822 culture compared to the group with 1% FBS and 2 ng/mL NGF (***Figure 5B***). Regarding the
823 SYN gene expression (***Figure 5C***), a statistically significant increase was observed after 7 days
824 of culture in the presence of 1% FBS and the growth factor mix, compared to almost all other
825 samples (except the 10% FBS control). The expression of the 100b gene significantly decreased
826 in cells cultured with 1% FBS and a growth factor mix for both 7 and 14 days, compared to
827 cells cultured with 1% FBS supplemented with 1% FBS and 2 ng/mL NGF (***Figure 5D***).
828 Analysis of MAP2 expression (***Figure 5E***) indicated a statistically significant increase in
829 expression in cultures with 1% FBS and 10 ng/mL GDNF compared to the 10% FBS control
830 group. After 14 days of culture, expression levels were further increased.
831 Immunocytochemical (ICC) detection of markers typical for mature neurons (MAP2)
832 and synapses (SYP) revealed differences in the number of MAP2/SYP+ positive cells,
833 depending on the growth factors used (***Figure 5F***). After 7 days of treatment with growth
834 factors, the highest percentage of MAP2/SYP+ cells was observed with VEGF (66%), and the
835 lowest with GDNF (44%). For MIX1 and MIX2, the results were 60% and 82%, respectively
836 (***Figure 5G***). After 14 days, all groups showed an increase in the percentage of positive cells,
837 with MIX1 and MIX2 still achieving the highest values—96% and 100%, representing an
838 increase of 36% and 18%, respectively, compared to day 7 (***Figure 5G***). When comparing both
839 time points, the largest increase in the percentage of positive cells was seen in the MIX1 (36%

840 increase) and MIX2 (18% increase) groups, which correlates with the PCR results. The analysis
841 of neurite length in cells treated with various growth factors over 7 and 14 days reveals
842 significant differences, particularly with MIX1 and MIX2. After 7 days, the average neurite
843 length was highest in the MIX1 group (59.3 μm), followed closely by MIX2 (57.3 μm), while
844 the control and other growth factors like NGF and GDNF showed lower average lengths,
845 ranging from 41.4 μm to 53.7 μm (***Figure 5H***). After 14 days, MIX1 and MIX2 exhibited
846 further growth, with MIX2 showing the most extended neurites (154.3 μm) compared to other
847 groups (***Figure 5I***). The average neurite length in the MIX1 group was also significantly higher
848 (133.6 μm) compared to the control (60.7 μm) and other growth factors like VEGF and NGF.
849 These results indicate that MIX1 and MIX2 promote substantial neurite extension, with MIX2
850 demonstrating the most pronounced effect over the 14 days (***Figure 5I***). From these results, we
851 concluded that MIX2 (containing 10 ng/mL NGF, 10 ng/mL GDNF, and 50 ng/mL VEGF.)

852 provides the most suitable migration and neurite outgrowth of the F11 DRG neural cells, and

853 hence fixed it for further studies.

854

855 **3.5. Morphological changes of F11 DRG neural cells under PEMF**

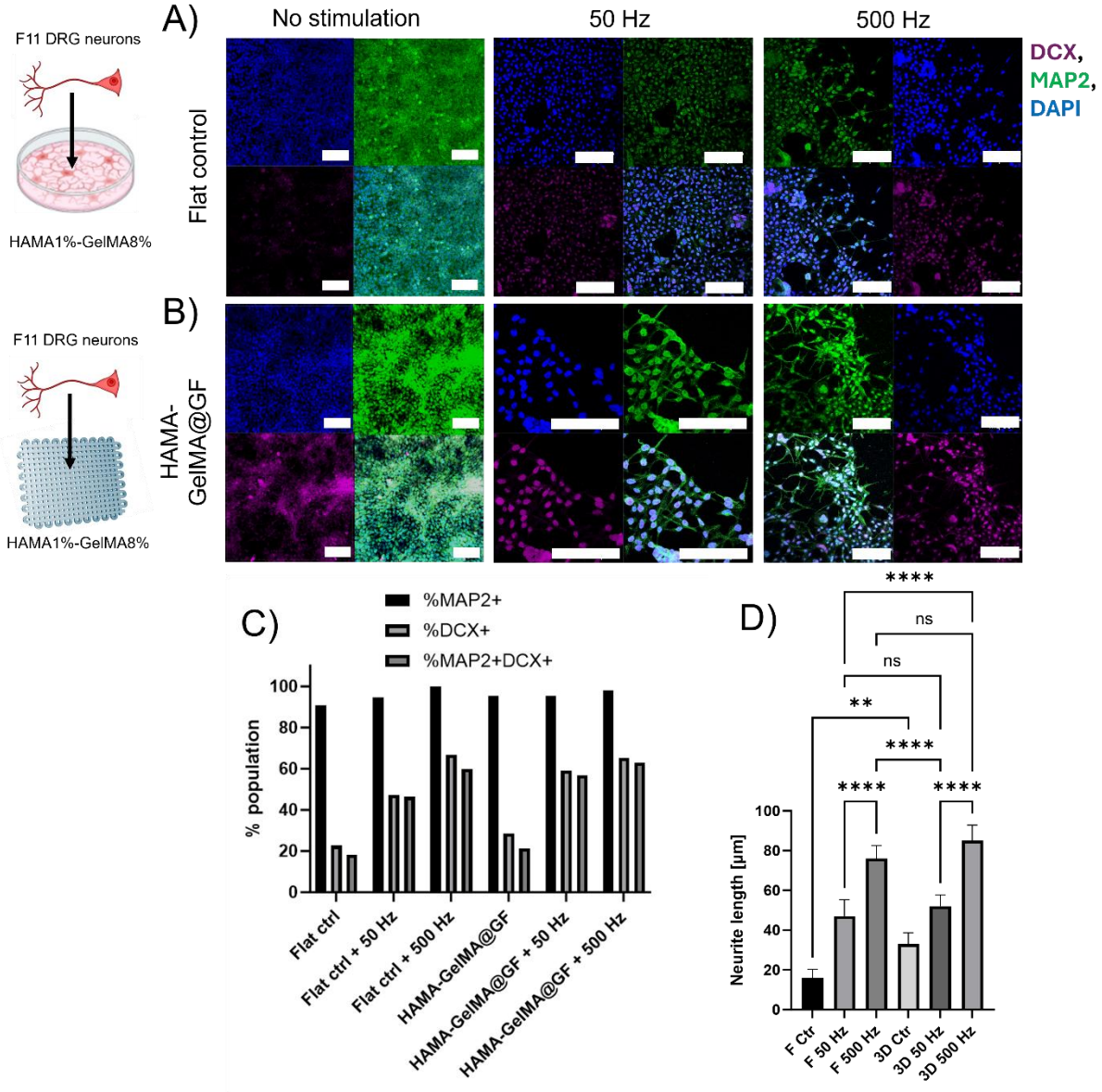


856

857 ***Figure 6:*** *Representative confocal images of F11 DRG neural cells cultured on A) flat control*

858 *Lab-Tek and B) HAMA1%-GelMA8%-GF(MIX2) cultured in control conditions and subjected*

859 *to 50 Hz or 500 Hz PEMF. Cells were immunostained for MAP2 (mature neurons; green) and*

860 *DCX (a marker of migrating neurons, violet). Cells were exposed to AC at 50 Hz and 500 Hz*

861 *for 3 days. The scale bar represents 100 µm in all images. C) The histograms show the %*
862 *population of MAP2, DCX and double MAP2/DCX positive cells at various frequencies, D)*
863 *Neurite length of F11 DRG neural cells. Statistical analysis was performed using One-Way*
864 *ANOVA (performed in GraphPad software) with three biological replicates. Data are*
865 *presented as mean ± standard deviation; *p<0.05, **p<0.01, ***p<0.001, ****p<0.0001.*
866
867 Non-invasive therapies like PEMF offer exciting potential for advancing nerve repair
868 strategies. PEMF has been shown to promote neurite extension, enhance neural cell viability,
869 and reduce inflammation, positioning it as a powerful adjunct to material-based interventions.
870 The combination of these approaches seems to address current limitations and offer ways to
871 achieve superior outcomes in nerve repair.[34] Before testing developed ***GrooveNeuroTube***,
872 we sought to find the optimal parameters for applying PEMF. We first conducted PEMF
873 stimulation for 3 days on flat control substrates (standard Lab-Teks substrates) and cells
874 cultured on hydrogels using an in-house PEMF stimulation system (***Figure S7***). We chose 50
875 and 500 Hz sinusoidal shape functions for experiments, providing a 0.24 mT alternating
876 magnetic field induction in the spectrum used across medical applications.[51, 52]
877 On day 3 of the culture, we performed ICC to detect the expression of DCX and MAP2 on
878 both control substrates as well as HAMA1%-GelMA8% composite hydrogel containing MIX2
879 of growth factors (named as HAMA1%-GelMA8%-GF) (***Figure 6 A, B***). The data shows that
880 exposure to PEMF (both 50 Hz and 500 Hz) significantly influences neural cell markers
881 (MAP2, DCX, and MAP2/DCX) in both 2D (Flat) and 3D (HAMA-GelMA@GF) cultures. In
882 the 2D system, PEMF 500 Hz treatment led to a percentage increase in MAP2-positive cells
883 from 94.7% to 100%, compared to PEMF 50 Hz (***Figure 6C***). Similarly, DCX-positive cells
884 increased from 47.4% to 66.7% (***Figure 6 A, C***). In the 3D HAMA-GelMA@GF environment,
885 the response to PEMF treatment was more pronounced. PEMF 500 Hz resulted in in an increase

886 in MAP2+ cells from 95.5% to 97.8%, and DCX+ cells from 59.1% to 65.2%compared to
887 PEMF 50 Hz (***Figure 6 B, C***). These findings suggest that the synergistic combination of the
888 3D hydrogel scaffold and PEMF, especially at 500 Hz, significantly enhances neural marker
889 expression compared to 2D conditions, indicating improved neural differentiation and
890 migration. The highest percentage of double-positive MAP2+DCX+ cells was found in the
891 HAMA-GelMA@GF + 500 Hz condition (63.04%), further supporting the enhanced
892 neurogenic commitment under this condition. More pronouncedly elongated MAP2/DCX+
893 cells were observed under the PEMF treatment condition (***Figure 6 A, B***). The highest number
894 of cells positive for both DCX and MAP2 was found at 500 Hz on Lab-Tek controls and flat
895 hydrogels (***Figure 6C***). Elongated cells with long neurites were observed on hydrogels
896 subjected to 50 and 500 Hz. The most extended neurites were found at 500 Hz, with neurites
897 reaching over 80 µm in length (***Figure 6D***). We also confirmed the cell viability after culture
898 and treatment with PEMF at two selected frequencies (50 and 500 Hz) for 24 hours. Cells were
899 cultured on 96-well plates, with substrates including HAMA, GelMA, HAMA1%-GelMA8%,
900 and PCL-HAMA1%-GelMA8% (unrolled ***GrooveNeuroTube***). The PEMF stimulation did not
901 negatively affect cell viability, with an average of 10% more cells showing improved viability
902 after PEMF stimulation than those cultured without stimulation (***Figure S8***). We chose the
903 square 500 Hz condition for further experiments based on the data because it demonstrated the
904 highest cell viability, particularly in the PCL-HAMA-GelMA group, where cell viability
905 reached 99.26 ± 0.9% at 500 Hz. In comparison, the viability for PCL-HAMA-GelMA at 50
906 Hz was significantly lower, at 74.1 ± 0.66%. This marked improvement in cell viability at 500
907 Hz made it the optimal experimental condition for further studies. From these preliminary tests,
908 we selected this stimulation to study our ***GrooveNeuroTube ex-vivo*** model over a prolonged
909 60-day period in the final stages.
910

### 3.6. Translation of 3D cell-laden collagen hydrogel in *GrooveNeuroTube* toward better *in vivo* resemblance

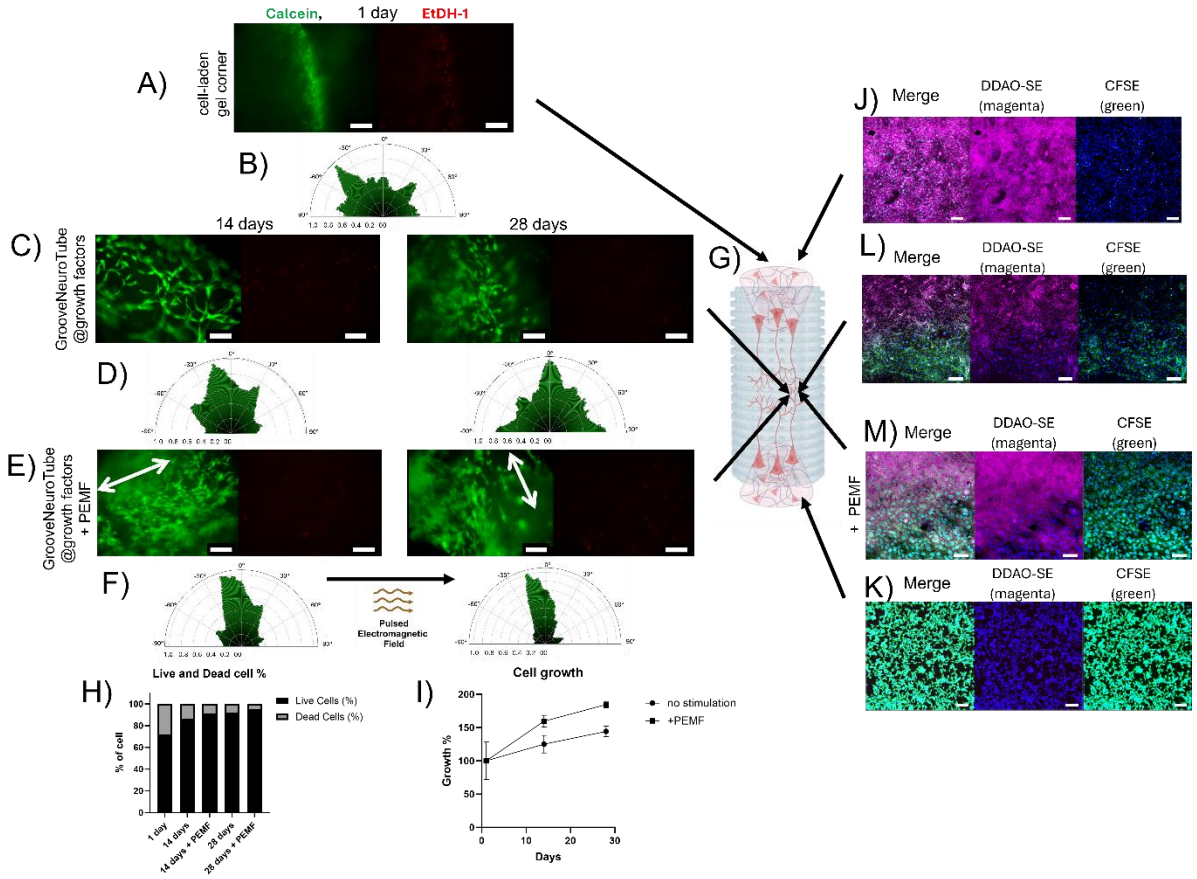


***Figure 7:*** *Confocal images of live/cell assay of live (Calcein-AM labelled; green) and dead (EtDH-1, red) neural cells cultured in 3D bioprinted tubes at the ends of the* ***GrooveNeuroTube*** *for A) 1, B) 14 and D) 28 days. Cells were exposed to PEMF magnet stimulation according to the parameters selected in previous experiments (PEMF) = AC 500 Hz. B, D, F) Circular histograms for the orientation of the cells direction, after culturing for 1, 14 and 28 days in* ***GrooveNeuroTube*** *cultured in standard conditions C) and E) subjected to PEMF. G) Scheme of the cross-section place, H) % of live and dead cells, I) % of cell growth with and without PEMF; J–M) Confocal images of DRG neurons bioprinted in collagen-mTG within the GrooveNeuroTube and labeled with fluorescent cell trackers. J) Neurons on the*

925 *upper side of the tube labeled with CellTrace™ Far Red DDAO-SE (magenta). K) Neurons on*
926 *the lower side of the tube labeled with CellTrace™ CFSE (green). L–M) Cross-sectional views*
927 *of the middle part of the tube after 28 days in culture: L) without PEMF stimulation and M)*
928 *with PEMF stimulation. Channels are shown individually; the absence of signal in one channel*
929 *reflects selective labeling of cells with a single fluorophore. The scale bar represents 100 µm*
930 *in all panels. The scale bar represents 100 µm in all images.*
931
932 To evaluate the ***GrooveNeuroTube*** (containing HAMA1%-GelMA8%-GF), we
933 performed a 3D bioprinting of F11 DRG neural cells on both ends of the tube to simulate *ex*
934 *vivo*-like conditions (***Figure 1C***). Experiments were conducted under standard culture
935 conditions and under conditions subjected to PEMF stimulation, selected as 500 Hz, as
936 described in the previous section. Cross-sections of the tube were made by vibratome cutting,
937 which allowed for accurate sectioning of 500 µm slices of the desired areas on days 1, 14, and
938 28 of culture. It can be observed that at the corner of the gel after 1 day of culture (***Figure 7A***,
939 arrow pointing at a schematic location of the tube), according to the design, there is a clear
940 distinction between cells labelled in the collagen hydrogel versus empty area of the tube. The
941 distributions of cell orientation angles indicate random directional growth on day 1 (***Figure***
942 ***7B***). In the central part of the tube (black arrows guiding locations in ***Figure 7G***), after 14 and
943 28 days, living cells labelled with Calcein-AM are visible, and their numbers increased with
944 each week of culture (***Figure 7H***). The cells are evenly and randomly ***(Figure 7D***) distributed
945 within the hydrogel in the 14 days of culture. In the case of the PEMF-treated group, we
946 observed more cells within the central location, and they were aligned in the direction of the
947 tube compared to the cells without PEMF (***Figure 7F***). After 28 days, a clear presence of many
948 live cells and a high ratio of live-to-dead cells were observed (***Figure 7H***). In the case of
949 ***GrooveNeuroTubes*** cultured for 28 days without PEMF, the cells showed only slight

950 organization within the hydrogel (***Figure 7D***). However, for samples subjected to PEMF, the
951 cells were organized along the tube exposed to PEMF (***Figure 7F***). Cell viability results
952 showed that, on day 1, 71.72 ± 0.28% of the cells were live, increasing to 86.67 ± 0.33% by
953 day 14 (***Figure 7H***). After PEMF exposure on day 14, live cells reached 91.21 ± 0.08%, and
954 by day 28, 92.02 ± 0.07% of the cells were alive. For samples exposed to PEMF for 28 days,
955 live cell viability improved further to 95.05 ± 0.05%, significantly reducing dead cells (4.95%
956 ± 0.05%) (***Figure 7H***). We could conclude that up to 28 days of culture, the PEMF stimulation
957 already shows beneficial signs for the growth of neural cells. To determine whether cells seeded
958 from both ends of the GrooveNeuroTube migrated and converged in the central region after 28
959 days in culture, we performed differential fluorescent cell labeling at each end of the conduit.
960 Specifically, cells seeded at one end were labeled with CellTrace™ Far Red DDAO-SE,
961 enabling detection in the far-red channel (***Figure 7J***), while cells seeded at the opposite end
962 were labeled with CellTrace™ CFSE, which is excited at 488 nm and detected in the green
963 channel (emission ~517 nm) (***Figure 7K***). After 28 days of culture, fluorescence imaging
964 revealed clear co-localization of both cell populations in the central part of the conduit,
965 indicating successful bidirectional migration and convergence (***Figure 7L-M***). Cells from both
966 ends migrated approximately 8.25 mm each, meeting at the center of the ~16.5 mm-long tube.
967 This experiment confirms symmetric migration dynamics and complete bridging of the conduit
968 by day 28. In the central region of the GrooveNeuroTube, differences could be observed
969 between the PEMF-stimulated and non PEMF-stimulated conditions. In particular, a higher
970 density of cells was detected under PEMF stimulation, enhancement of proliferation and
971 survival (***Figure 6I***). These findings align with previous reports showing that pulsed
972 electromagnetic fields (PEMF) promote both neurite outgrowth and proliferation in neuronal-
973 like cell lines, including F11 cells, which are derived from dorsal root ganglia. In our system,
974 we also observed that, consistent with previous findings in other experimental conditions, cells

exhibited longitudinal alignment along the axis of the conduit, a phenomenon further supported by the presence of directional neurite extension (***Figure 6M***). This alignment is likely influenced by both the architectural guidance of the mesh structure and the directional cues enhanced by PEMF exposure.

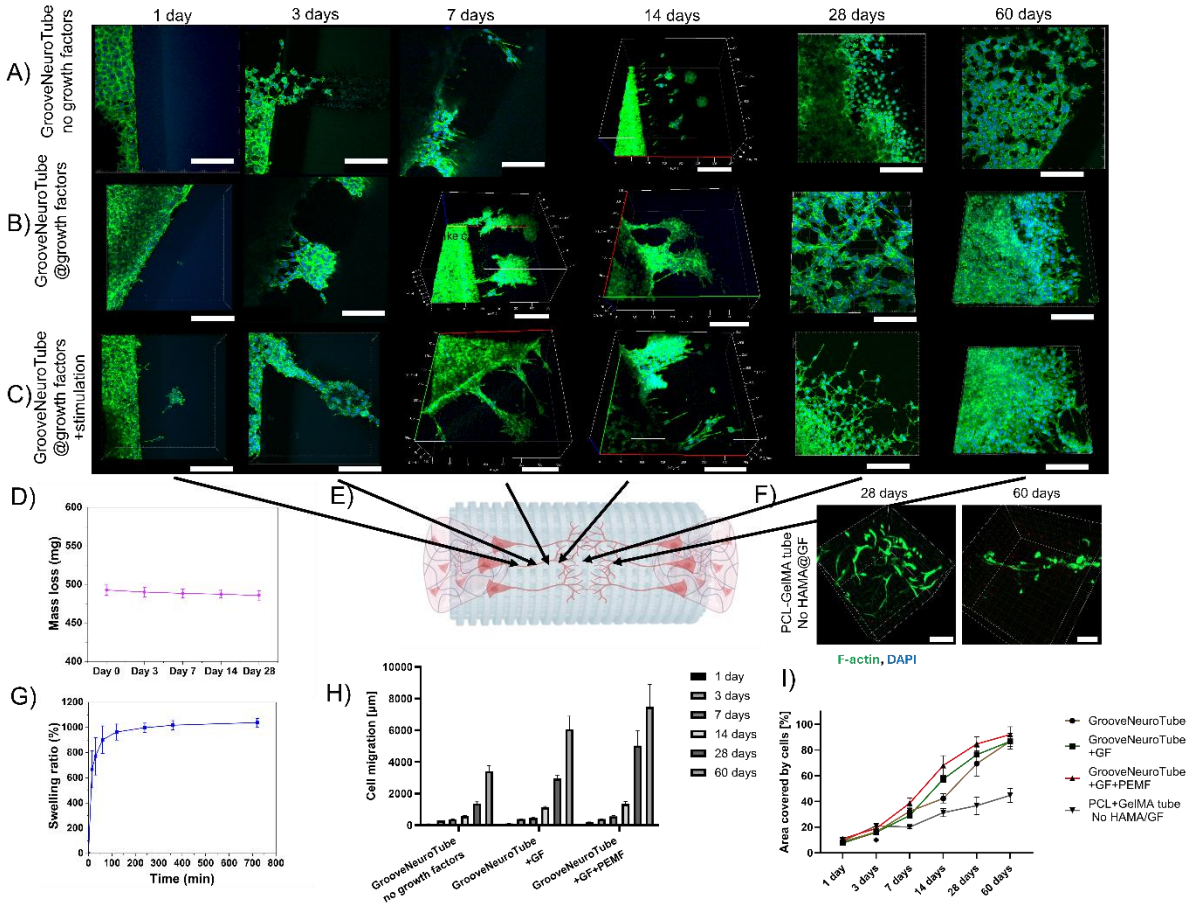


***Figure 8:*** *Representative confocal images of stained F-actin cytoskeleton (green, Pallodin) and nucleus (blue, DAPI) in F11 DRG neural cells 3D bioprinted at the end of the: A) HAMA1%-GelMA8% without growth factors, B) HAMA1%-GelMA8% with growth factors (**GrooveNeuroTube**), C) HAMA1%-GelMA8% with growth factors (**GrooveNeuroTube**) + PEMF, D) Degradation of GrooveNeuroTube, E) Schematic representation of the crossection, F) Tube made of only PCL and GelMA8% as control, after 28 and 60 days in culture stained for F-actin cytoskeleton (green, Phalloidin) and nucleus (blue, DAPI). The scale bar in each*

987 *image represents 100 µm., G) Swelling ratio, H) Cell migration analysis, I) Total area covered*
988 *by cells. The scale bar represents 100 µm in all images.*
989
990 Next, to assess whether cell migration is influenced solely by PEMF, we tested our
991 ***GrooveNeuroTube*** again with or without the addition of growth factors (***Figure 8***). These were
992 tested over a period of 1 to 60 days under long-term conditions to stimulate *ex vivo* experiments
993 and reduce *in vivo* testing on animals. The results revealed that in all conditions, F11 DRG
994 neural cells were able to migrate to the centre of the tube over a period of 28-60 days. This was
995 confirmed by performing transverse cross-sections at 28 and 60 days, followed by ICC testing,
996 which identified the cells (***Figure 7C, E*** and ***8A, B, C, F, G***). We observed elongated cells and
997 multicellular clusters migrating from the cell-laden hydrogel segments that were 3D bioprinted
998 at both ends of the tubular scaffold. Migration distance was determined by measuring the extent
999 of these advancing clusters, which emerged from the hydrogel regions and progressed along
1000 the inner surface of the tube toward the central region. The most remarkable cell migration was
1001 noted for the ***GrooveNeuroTube*** containing growth factors and under PEMF stimulation
1002 (***Figure 8C, G***). The data reveals that cell migration varied depending on the conditions
1003 applied, mainly when active agents and PEMF were used. The migration distance in the
1004 GrooveNeuroTube without growth factors group ranged from 0.074 mm on day 1 to 3.52 mm
1005 on day 60 (***Figure 8G***). The ***GrooveNeuroTube+GF*** group showed higher migration, with
1006 distances starting at 0.1064 mm on day 1 and reaching 5.46 mm by day 60 (***Figure 8G***). The
1007 ***GrooveNeuroTube+GF+PEMF*** group demonstrated the highest migration, with cells
1008 migrating 0.1 mm on day 1 and extending up to 7.2 mm on day 60. For the
1009 ***GrooveNeuroTube+GF+PEMF*** group, the average migration across all time points was
1010 3.7926 ± 1.3039 mm. The highest observed migration was 7.2 mm at day 60, representing an
1011 impressive 88% greater migration than the ***GrooveNeuroTube+GF*** group, and 106% more

1012 than the ***GrooveNeuroTube*** group. On average, cells in the ***GrooveNeuroTube+GF+PEMF***
1013 group migrated 3.79 ± 1.30 mm, which is a notable improvement compared to the 2.72 ± 1.46
1014 mm in the ***GrooveNeuroTube+GF*** group and 1.39 ± 0.93 mm in the ***GrooveNeuroTube*** group.
1015 These results indicate that PEMF, in combination with active agents, significantly enhanced
1016 cell migration (***Figure 8G***). On day 60, most of the observed cells were dispersed throughout
1017 the entire volume of the construct, indicating that they had colonized nearly the whole structure.
1018 To confirm this, an analysis of the area covered by cells was performed. The highest cell density
1019 on day 60 was indeed observed in the PEMF-treated group (***Figure 8C***). The results
1020 demonstrate that the ***GrooveNeuroTube+GF+PEMF*** exhibited the highest cell coverage area
1021 at all time points, showing a marked increase over the duration of the experiment. Starting at a
1022 relatively low level on day 1, the cell coverage in this group grew significantly, reaching 95 ±
1023 7% on day 60, representing an increase of approximately 850%. This suggests combining
1024 growth factors and PEMF greatly enhances cell migration over time (***Figure 8C***). The
1025 ***GrooveNeuroTube+GF*** group also showed a steady increase in cell coverage, starting at 7-10
1026 on day 1 and rising to 88 ± 6 % by day 60, corresponding to a 700% increase (***Figure 8B***). This
1027 indicates that growth factors alone have a considerable impact on promoting cell migration,
1028 although the effect is less pronounced compared to the group with PEMF. In contrast, the
1029 PCL+GelMA tube - No HAMA@GF control group consistently demonstrated the lowest cell
1030 coverage area across all time points, indicating the importance of both components in
1031 composite hydrogel for the therapeutical effect. Initially, this group started with a cell coverage
1032 of 6-12 on day 1, and although there was some growth over time, it only reached 39 ±4 % by
1033 day 60, which represents a 550% increase (***Figure 8A***). This lower growth rate suggests that
1034 the absence of growth factors and PEMF results in a less efficient cell migration process. In
1035 summary, the data clearly shows that the combination of growth factors + PEMF leads to the
1036 most significant and sustained increase in cell coverage, indicating a potent synergistic effect

1037 on cell migration. Meanwhile, the growth factors alone have a notable but comparatively more
1038 minor impact, and the PCL+GelMA tube - No HAMA@GF group demonstrated the least
1039 response, highlighting the importance of both growth factors and PEMF in promoting cell
1040 migration (***Figure 8H***). This proved that the F11 DRG neural cells could freely migrate within
1041 the developed hydrogel composition and that the additional PEMF stimulation enhanced their
1042 migration.
1043 The swelling ratio of HAMA1%-GelMA8% hydrogel shown in ***Figure 8G*** indicate absorption
1044 ~1000% its dry weight indicating high water retention capability. The degradation (***Figure 8D***)
1045 of the GrooveNeuroTube shows steady and minimal mass loss of ~2% over 60 days indicates
1046 excellent structural stability under physiological environment. The PCL microfibers ensure
1047 long-term stability, while the hydrogel enhances bioactivity and supports cell migration and
1048 axonal regrowth. Unlike solid-walled PCL-based conduits with slow degradation [1,3,4], our
1049 fibrous architecture offers controlled support without long-term tissue persistence.**3.7.**
1050 **Characterization of neurites**

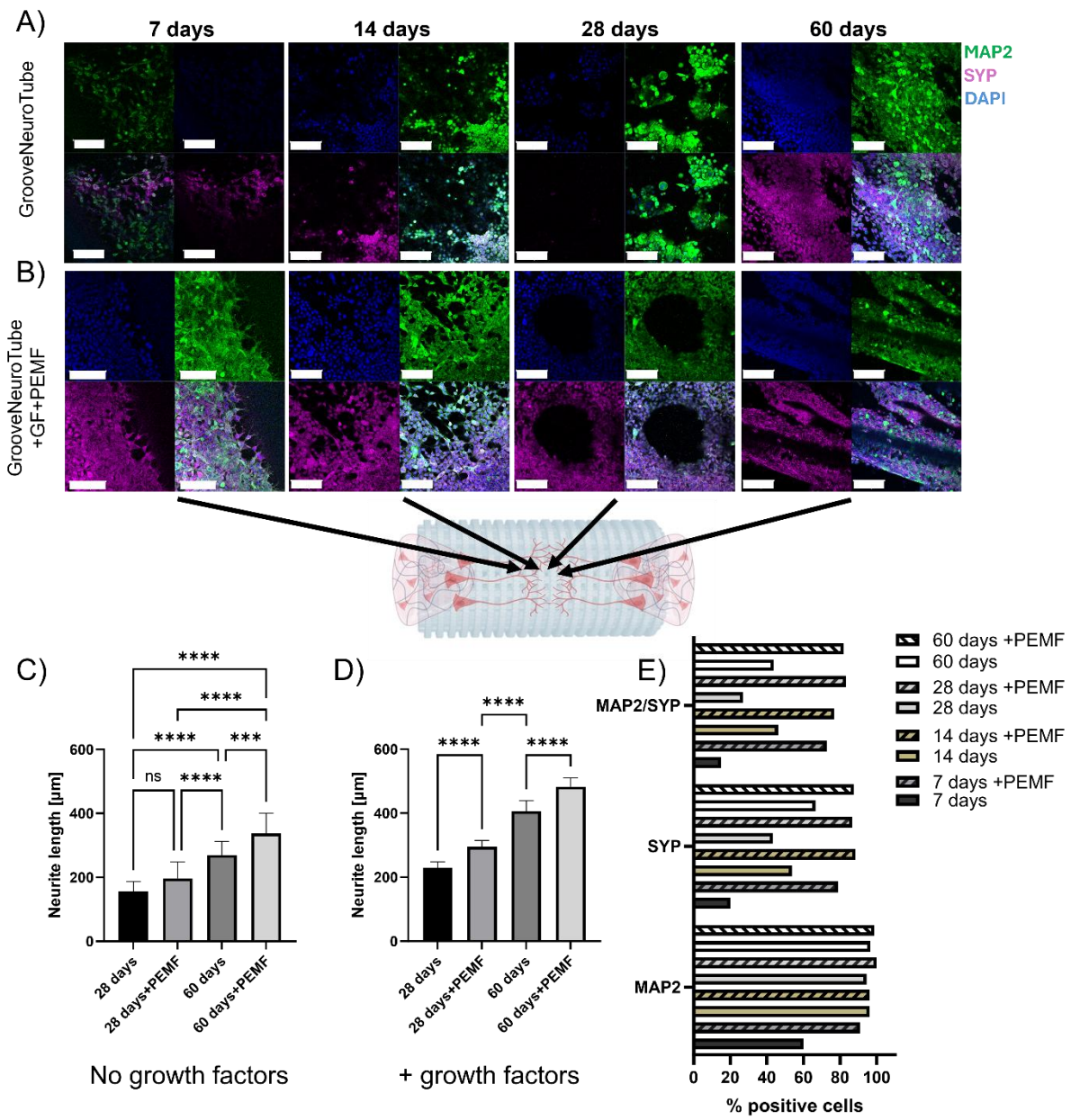


***Figure 9:*** *Confocal images of F11 DRG neural cells under 7, 14, 28, and 60 days in culture, immunostained for MAP2 (mature neurons; green) and SYP (synaptic marker, violet). A) The upper panel shows cell orientation within the* ***GrooveNeuroTube+GF*** *and B) The bottom panel presents cell orientation after exposure to PEMF (****GrooveNeuroTube+GF+PEMF****). The scale bar represents 100 µm in all images. C) Mean neurite length of neural cells cultured for 28 and 60 days within a tube without growth factors, D) Mean neurite length cultured for 28 and 60 days within a tube with growth factors. For both C and D cases with and without PEMF stimulation are presented. The population means (represented by each bar) essentially differ*

1060 *at the significance level - 0.01. E) The histograms show the quantification of the number of*
1061 *positive /total number of cells corresponding to MAP2/SYP+; the asterisk indicates significant*
1062 *differences at p < 0.01; ****p<0.0001. ANOVA*
1063
1064 To confirm the functional process of neuronal maturation, we performed ICC to
1065 determine the presence of MAP2 and SYP proteins, characteristic of synaptic vesicles, which
1066 are considered synaptic markers, over 60 days of culture. After 7 days of culture, a significant
1067 proportion of the MAP2/SYP+ cells with an elongated shape were present on the PEMF-treated
1068 tube, compared to the sample without growth factors and PEMF (***Figure 9***). However, starting
1069 from day 7, highly elongated MAP2/SYP+ cells, closely adjacent to each other, with a strong
1070 SYP fluorescence signal found at their intercellular junctions, were observed after 7, 14, 28,
1071 and 60 days of culturing under PEMF conditions. These cells were kept nearby, presumably
1072 allowing inter-cellular connections. Cells cultured within the tube without active agents and
1073 PEMF surfaces (***Figure 9A***) were DCX/MAP2/SYP+. However, the cells' shape was not
1074 polarized and did not resemble those grown on PEMF, as their neurites were shorter than the
1075 cells cultured (***Figure 9B***). The results of the analysis show a clear impact of growth factors
1076 (GF) and PEMF stimulation on the expression of neuronal markers, particularly MAP2, SYP,
1077 and their co-expression (MAP2/SYP), over time. In conditions without growth factors (-GF),
1078 the percentage of MAP2-positive cells increases steadily from 60% at 7 days to nearly 100%
1079 by 60 days, suggesting progressive neuronal differentiation without external growth signals
1080 (***Figure 9 E***). However, the expression of SYP, a marker for synaptic proteins, is considerably
1081 lower under -GF conditions, starting at 20% on day 7 and fluctuating across time points,
1082 peaking at 86.67% on day 28 before slightly declining to 66.67% on day 60. The co-expression
1083 of MAP2/SYP in -GF conditions is also relatively low, with an initial value of 15% on day 7,
1084 rising to 83.33% by day 28, but dropping back to 43.86% by day 60. In contrast, the conditions

1085 with growth factors and PEMF (***GrooveNeuroTube+GF+PEMF***) (***Figure 9B***) led to a marked
1086 increase in the percentage of MAP2-positive cells throughout the experiment. Starting at
1087 90.91% on day 7, the percentage continued to increase, reaching 98.63% by day 60. This
1088 suggests that combining GF and PEMF significantly enhances neuronal differentiation and
1089 maturation. SYP expression in these conditions was also significantly higher than in the -GF
1090 group, beginning at 78.79% on day 7, peaking at 88.46% by day 14, and stabilizing around
1091 87.67% at day 60. The MAP2/SYP co-expression followed a similar trend, starting at 72.73%
1092 on day 7, rising to 76.92% by day 14, and reaching 82.19% by day 60, indicating that GF and
1093 PEMF treatment promotes not only neuronal differentiation but also synaptic maturation over
1094 time ***(Figure 9 E).*** The data reveals a time-dependent effect of growth factors and PEMF on
1095 neuronal marker expression. While MAP2 expression continues to increase in both the -GF
1096 and GF+PEMF conditions, growth factors and PEMF consistently result in higher levels of
1097 MAP2, SYP, and MAP2/SYP co-expression, especially at later time points. In particular, the
1098 GF+PEMF condition enhanced synaptic protein expression (SYP) and neuronal maturation
1099 (MAP2/SYP co-expression) more effectively than -GF conditions, demonstrating the
1100 combined positive impact of growth factors and PEMF on neuronal development and synaptic
1101 protein expression.

1102 Next, we analysed the neurites' outgrowth of F11 DRG neural cells within the tube for 28
1103 and 60 days with conditions without and with PEMF (***Figure 9C, D***). Consecutively, we
1104 examined the average length of the neurites. With and without stimulation, DRG neural cells
1105 cultured within ***GrooveNeuroTube*** showed significant differences in neurite length (***Figure***
1106 ***9C***). The average length of neurites in ***GrooveNeuroTube*** without active agents and without
1107 PEMF after 28 days was 156 ± 29 µm, whereas in the PEMF-treated sample, the average
1108 neurite length was 196 ± 49 µm. The average length of neurites after 28 days within the tube
1109 with growth factors and PEMF was 229 ± 18 µm and 295 ± 19 µm in the tube with PEMF. On

1110 the 60th day, it was 406 ± 32 μm in the ***GrooveNeuroTube*** with active agents without PEMF
1111 and 482 ± 27 μm in the ***GrooveNeuroTube*** with PEMF (***Figure 9C, D***).
1112

1113 **3.8. Antibacterial effects of GrooveNeuroTube**

1114 To finally demonstrate another possibility for future studies on our ***GrooveNeuroTube,*** we
1115 briefly demonstrate the encapsulation of lysozyme, a known antimicrobial agent.[53] We
1116 studied its effects over a more extended period of time (up to 21 days) against *S. aureus* and *E.*
1117 *coli*. To do so, we loaded lysozyme within HAMA1%-GelMA8% hydrogel and examined
1118 bacterial inhibition over 7, 14, and 21 days. Detailed results are described in the supplementary
1119 materials. The lysozyme solution alone (Lyz 0.5 mg/mL) demonstrated moderate antibacterial
1120 effects. Still, the GelMA-HAMA-Lyz hydrogel was more effective in reducing bacterial
1121 growth over time to inhibit over 80% of the bacteria within 21 days (***Figure S9***). These results
1122 indicate the sustained antibacterial potential of the GelMA-HAMA-Lyz hydrogel against *E.*
1123 *coli* (***Figure S9D***). The F11 neural cells treated with lysozyme for 24 (***Figure S10***), 48 (***Figure***
1124 ***S11***), and 72 (***Figure S12***) hours showed no evident toxic effect on F11 DRG neural cells. Cell
1125 morphology under each condition was compared to the untreated control conditions, and no
1126 significant morphological changes were observed, indicating that lysozyme treatment did not
1127 induce toxicity at any of the time points analysed. This confirms that the ***GrooveNeuroTube***
1128 construct can be used to study the effects of antibacterial agents and mimic infection-like
1129 scenarios in future studies.
1130

1131 **4. Conclusions**

1132 This study aimed to demonstrate the practicality of using PCL grid substrates with
1133 internal fibers to create tubes with topographical cues. This structure protects the composite
1134 hydrogel we developed, containing HAMA1%-GelMA8% and active agents such as a mix of

growth factors or the antimicrobial enzyme lysozyme. The rolled tube is a stable construct that could serve as a neurotube, promoting the regeneration of peripheral nerves. Additionally, we developed 3D bioprinting of collagen-cell-laden hydrogels on both ends of the tubes to imitate the growth of DRG neurons after injury. This developed *ex vivo*-like model could serve as a platform to stimulate neural regeneration by studying DRG migration or, in the future, other cell types or their combinations. We effectively demonstrated possibilities to study neural cell behaviour on these bioprinted constructs with and without loaded growth factors, with the influence of PEMF over a prolonged amount of time, and even the possibility to incorporate antimicrobial agents to study anti-infective strategies. The unique composition of the fibrous tubular architecture, composite hydrogel, growth factor composition, and PEMF enhanced D11 DRG neuron migration, neurite outgrowth, and cell-cell interaction, supporting their maturation and proving similar effects observed in *vivo* studies by others.[34] We expect our G***rooveNeuroTube*** model to be broadly applicable for future neural tissue developmental and regeneration studies and demonstrate its potential as an effective new graft for peripheral nerve repair.

**Funding sources**

The authors acknowledge financial support from the Small Grant Scheme 2020 (Norway Grants) from the National Centre for Research and Development (NOR/SGS/GrooveNeuroTube/0321/2020-00) (neurotube research) and from the National Science Centre (NSC) grant (2022/47/D/ST5/03467) (3D bioprinting research).

JCRC is grateful for funding from the Spanish Government (grant PID2022-137484OB-I00 funded by MCIN/AEI/ 10.13039/501100011033 and by ERDF, EU), from the Department of Education, *Junta de Castilla y León* (grant VA188P23 and CLU-2023-1-05 cofunded by

ERDF, EU) and from *Centro en Red de Medicina Regenerativa y Terapia Celular de Castilla y León*.

**Acknowledgements**

We are grateful to Dr. Abhishek Indurkar (Center for Advanced Technologies, Adam Mickiewicz University) for performing FTIR measurements and for his valuable contribution to the analysis of FTIR, NMR spectra, and swelling test results.

**CRediT authorship contribution statement**

**J.L.**: Conceptualization, data curation, formal analysis, funding acquisition, investigation, methodology, project administration, resources, supervision, validation, visualization, co-writing - original draft. **Y.R.:** Writing – original draft, Validation, Methodology, Formal analysis. **H.I.:** Writing, Methodology, Investigation, Data curation. **A.O.:** Writing, Methodology, Investigation, Data curation. **Ł.P.:** Writing, Methodology, Investigation, Data curation. **K.F.:** Writing, Methodology, Investigation, Data curation. **J.C.R.C.:** Writing, Methodology, Investigation, Data curation. **J.K.W.**:, Formal analysis, methodology, validation, visualization, co-writing - original draft; **K.T**.: Writing, Methodology, Investigation, visualization, Data curation.

**Notes**

The authors declare no competing financial interest. All research data supporting this publication are directly available within this publication, as well as associated supporting information.

**ORCID numbers of authors**

**Jagoda Litowczenko:** https://orcid.org/0000-0002-8515-2171

**Yannick Richter:** https://orcid.org/0009-0008-9035-6137

**Hawrez Ismael**: https://orcid.org/0009-0007-7968-1521

**Łukasz Popenda:** https://orcid.org/0000-0003-1117-3081

**Adam Ostrowski:** https://orcid.org/0000-0002-3936-5184

**Katarzyna Fiedorowicz:** https://orcid.org/0000-0002-3921-8459

**Jose Carlos Rodrigez Cabello:** https://orcid.org/0000-0002-3438-858X

**Jacek K. Wychowaniec:** https://orcid.org/0000-0002-6597-5242

**Krzysztof Tadyszak:** https://orcid.org/0000-0002-0370-9766

## References

[1] R. López-Cebral, J. Silva-Correia, R.L. Reis, T.H. Silva, J.M. Oliveira, Peripheral Nerve Injury: Current Challenges, Conventional Treatment Approaches, and New Trends in Biomaterials-Based Regenerative Strategies, ACS Biomaterials Science & Engineering 3(12) (2017) 3098-3122.

[2] P. Arthur-Farraj, M.P. Coleman, Lessons from Injury: How Nerve Injury Studies Reveal Basic Biological Mechanisms and Therapeutic Opportunities for Peripheral Nerve Diseases, Neurotherapeutics 18(4) (2021) 2200-2221.

[3] X. Yao, T. Xue, B. Chen, X. Zhou, Y. Ji, Z. Gao, B. Liu, J. Yang, Y. Shen, H. Sun, X. Gu, B. Dai, Advances in biomaterial-based tissue engineering for peripheral nerve injury repair, Bioactive Materials 46 (2025) 150-172.

[4] B.J. Parker, D.I. Rhodes, C.M. O'Brien, A.E. Rodda, N.R. Cameron, Nerve guidance conduit development for primary treatment of peripheral nerve transection injuries: A commercial perspective, Acta Biomaterialia 135 (2021) 64-86.

[5] Z. Kočí, R. Sridharan, A.J. Hibbitts, S.L. Kneafsey, C.J. Kearney, F.J. O'Brien, The Use of Genipin as an Effective, Biocompatible, Anti-Inflammatory Cross-Linking Method for Nerve Guidance Conduits, Advanced Biosystems 4(3) (2020) 1900212.

[6] M. Sharifi, M. Kamalabadi-Farahani, M. Salehi, S. Ebrahimi-Barough, M. Alizadeh, Recent advances in enhances peripheral nerve orientation: the synergy of micro or nano patterns with therapeutic tactics, Journal of Nanobiotechnology 22(1) (2024) 194.

[7] J. Litowczenko, J.K. Wychowaniec, K. Załęski, Ł. Marczak, C.J.C. Edwards-Gayle, K. Tadyszak, B.M. Maciejewska, Micro/nano-patterns for enhancing differentiation of human neural stem cells and fabrication of nerve conduits via soft lithography and 3D printing, Biomaterials Advances 154 (2023) 213653.

[8] Y. Ma, H. Gao, H. Wang, X. Cao, Engineering topography: effects on nerve cell behaviors and applications in peripheral nerve repair, Journal of Materials Chemistry B 9(32) (2021) 6310-6325.

[9] E.C. Spivey, Z.Z. Khaing, J.B. Shear, C.E. Schmidt, The fundamental role of subcellular topography in peripheral nerve repair therapies, Biomaterials 33(17) (2012) 4264-4276.

[10] F. Liu, J. Xu, L. Wu, T. Zheng, Q. Han, Y. Liang, L. Zhang, G. Li, Y. Yang, The Influence of the Surface Topographical Cues of Biomaterials on Nerve Cells in Peripheral Nerve Regeneration: A Review, Stem Cells International 2021(1) (2021) 8124444.

[11] D. Hoffman-Kim, J.A. Mitchel, R.V. Bellamkonda, Topography, Cell Response, and Nerve Regeneration, Annual Review of Biomedical Engineering 12(Volume 12, 2010) (2010) 203-231.

1233 [12] K. Liu, L. Yan, R. Li, Z. Song, J. Ding, B. Liu, X. Chen, 3D Printed Personalized Nerve
1234 Guide Conduits for Precision Repair of Peripheral Nerve Defects, Advanced Science 9(12)
1235 (2022) 2103875.
1236 [13] B.P. Toole, Hyaluronan: from extracellular glue to pericellular cue, Nature Reviews
1237 Cancer 4(7) (2004) 528-539.
1238 [14] J.K. Wychowaniec, E.I. Bektas, A.J. Vernengo, M. Muerner, M. Airoldi, P.S. Tipay, J.
1239 Sapudom, J. Teo, D. Eglin, M. D'Este, Effect of molecular weight of tyramine-modified
1240 hyaluronan on polarization state of THP-1 and peripheral blood mononuclear cells-derived
1241 macrophages, Biomaterials Advances 169 (2025) 214166.
1242 [15] K. Salma-Ancane, A. Sceglovs, E. Tracuma, J.K. Wychowaniec, K. Aunina, A. Ramata-
1243 Stunda, V. Nikolajeva, D. Loca, Effect of crosslinking strategy on the biological, antibacterial
1244 and physicochemical performance of hyaluronic acid and varepsilon-polylysine based
1245 hydrogels, Int J Biol Macromol 208 (2022) 995-1008.
1246 [16] M. Halperin-Sternfeld, A. Pokhojaev, M. Ghosh, D. Rachmiel, R. Kannan, I. Grinberg,
1247 M. Asher, M. Aviv, P.X. Ma, I. Binderman, R. Sarig, L. Adler-Abramovich,
1248 Immunomodulatory fibrous hyaluronic acid-Fmoc-diphenylalanine-based hydrogel induces
1249 bone regeneration, J Clin Periodontol 50(2) (2023) 200-219.
1250 [17] W. Guo, L. Douma, M.H. Hu, D. Eglin, M. Alini, A. Secerovic, S. Grad, X. Peng, X. Zou,
1251 M. D'Este, M. Peroglio, Hyaluronic acid-based interpenetrating network hydrogel as a cell
1252 carrier for nucleus pulposus repair, Carbohydr Polym 277 (2022) 118828.
1253 [18] Q. Wei, Z. Jin, W. Zhang, Y. Zhao, Y. Wang, Y. Wei, X. He, G. Ma, Y. Guo, Y. Jiang, Z.
1254 Hu, Honokiol@PF127 crosslinked hyaluronate-based hydrogel for promoting wound healing
1255 by regulating macrophage polarization, Carbohydr Polym 303 (2023) 120469.
1256 [19] I.A. Hammam, R. Winters, Z. Hong, Advancements in the application of biomaterials in
1257 neural tissue engineering: A review, Biomedical Engineering Advances 8 (2024) 100132.

1258 [20] E.A. Mays, S.S. Kallakuri, H.G. Sundararaghavan, Heparin-hyaluronic acid nanofibers
1259 for growth factor sequestration in spinal cord repair, Journal of Biomedical Materials Research
1260 Part A 108(10) (2020) 2023-2031.
1261 [21] Y. Tabata, Y. Ikada, Protein release from gelatin matrices, Advanced Drug Delivery
1262 Reviews 31(3) (1998) 287-301.
1263 [22] J. Xu, Y. Xia, C.-D. Qiao, W. Zhu, Y. Wang, T.-D. Li, Solid-state structure of gelatin-
1264 mono epoxy terminated polydimethylsiloxane polymer: Effect of electrostatic and hydrophobic
1265 interactions, Colloids and Surfaces B: Biointerfaces 123 (2014) 945-950.
1266 [23] M.C. Gómez-Guillén, J. Turnay, M.D. Fernández-Díaz, N. Ulmo, M.A. Lizarbe, P.
1267 Montero, Structural and physical properties of gelatin extracted from different marine species:
1268 a comparative study, Food Hydrocolloids 16(1) (2002) 25-34.
1269 [24] A. Ito, A. Mase, Y. Takizawa, M. Shinkai, H. Honda, K. Hata, M. Ueda, T. Kobayashi,
1270 Transglutaminase-mediated gelatin matrices incorporating cell adhesion factors as a
1271 biomaterial for tissue engineering, J Biosci Bioeng 95(2) (2003) 196-9.
1272 [25] R.-N. Chen, H.-O. Ho, M.-T. Sheu, Characterization of collagen matrices crosslinked
1273 using microbial transglutaminase, Biomaterials 26(20) (2005) 4229-4235.
1274 [26] T. Chen, D.A. Small, M.K. McDermott, W.E. Bentley, G.F. Payne, Enzymatic methods
1275 for in situ cell entrapment and cell release, Biomacromolecules 4(6) (2003) 1558-63.
1276 [27] Y. Dong, S. Zhao, W. Lu, N. Chen, D. Zhu, Y. Li, Preparation and characterization of
1277 enzymatically cross-linked gelatin/cellulose nanocrystal composite hydrogels, RSC Advances
1278 11(18) (2021) 10794-10803.
1279 [28] M. Djabourov, P. Papon, Influence of thermal treatments on the structure and stability of
1280 gelatin gels, Polymer 24(5) (1983) 537-542.

1281 [29] Y. Liu, R. Weng, W. Wang, X. Wei, J. Li, X. Chen, Y. Liu, F. Lu, Y. Li, Tunable physical
1282 and mechanical properties of gelatin hydrogel after transglutaminase crosslinking on two
1283 gelatin types, International Journal of Biological Macromolecules 162 (2020) 405-413.
1284 [30] W. Ye, H. Li, K. Yu, C. Xie, P. Wang, Y. Zheng, P. Zhang, J. Xiu, Y. Yang, F. Zhang, Y.
1285 He, Q. Gao, 3D printing of gelatin methacrylate-based nerve guidance conduits with multiple
1286 channels, Materials & Design 192 (2020) 108757.
1287 [31] C.M. Walsh, J.K. Wychowaniec, D.F. Brougham, D. Dooley, Functional hydrogels as
1288 therapeutic tools for spinal cord injury: New perspectives on immunopharmacological
1289 interventions, Pharmacol Ther 234 (2022) 108043.
1290 [32] C.M. Walsh, J.K. Wychowaniec, L. Costello, D.F. Brougham, D. Dooley, An In Vitro and
1291 Ex Vivo Analysis of the Potential of GelMA Hydrogels as a Therapeutic Platform for
1292 Preclinical Spinal Cord Injury, Adv Healthc Mater 12(26) (2023) e2300951.
1293 [33] R.V. Haberberger, C. Barry, D. Matusica, Immortalized Dorsal Root Ganglion Neuron
1294 Cell Lines, Frontiers in Cellular Neuroscience 14 (2020).
1295 [34] F. Fontana, A. Cafarelli, F. Iacoponi, S. Gasparini, T. Pratellesi, A.N. Koppes, L. Ricotti,
1296 Pulsed electromagnetic field stimulation enhances neurite outgrowth in neural cells and
1297 modulates inflammation in macrophages, Engineered Regeneration 5(1) (2024) 80-91.
1298 [35] F. Vincenzi, A. Ravani, S. Pasquini, S. Merighi, S. Gessi, S. Setti, R. Cadossi, P.A. Borea,
1299 K. Varani, Pulsed Electromagnetic Field Exposure Reduces Hypoxia and Inflammation
1300 Damage in Neuron-Like and Microglial Cells, Journal of Cellular Physiology 232(5) (2017)
1301 1200-1208.
1302 [36] J.F. Cherry, N.K. Bennett, M. Schachner, P.V. Moghe, Engineered N-cadherin and L1
1303 biomimetic substrates concertedly promote neuronal differentiation, neurite extension and
1304 neuroprotection of human neural stem cells, Acta Biomaterialia 10(10) (2014) 4113-4126.

1305 [37] W.C. Low, W.W.Y. Yau, L.W. Stanton, G. Marcy, E. Goh, S.Y. Chew, Directing
1306 Neuronal Differentiation of Primary Neural Progenitor Cells by Gene Knockdown Approach,
1307 DNA and Cell Biology 31(7) (2012) 1148-1160.
1308 [38] J. Litowczenko, B.M. Maciejewska, J.K. Wychowaniec, M. Koscinski, S. Jurga, A.
1309 Warowicka, Groove-patterned surfaces induce morphological changes in cells of neuronal
1310 origin, J Biomed Mater Res A 107(10) (2019) 2244-2256.
1311 [39] J. Amirian, J.K. Wychowaniec, M. D′Este, A.J. Vernengo, A. Metlova, A. Sizovs, A.
1312 Brangule, D. Bandere, Preparation and Characterization of Photo-Cross-Linkable
1313 Methacrylated Silk Fibroin and Methacrylated Hyaluronic Acid Composite Hydrogels,
1314 Biomacromolecules 25(11) (2024) 7078-7097.
1315 [40] T. Bedir, D. Baykara, A. Sahin, I. Senel, E. Kaya, G.B. Tinaz, O. Gunduz, C.B. Ustundag,
1316 Development of Specially Designed Nanoparticle-coated 3D-printed Gelatin Methacryloyl
1317 Patches for Potential Tissue Engineering Applications, Macromolecular Materials and
1318 Engineering n/a(n/a) (2024) 2400199.
1319 [41] S. Paul, K. Schrobback, P.A. Tran, C. Meinert, J.W. Davern, A. Weekes, T.J. Klein, Photo-
1320 Cross-Linkable, Injectable, and Highly Adhesive GelMA-Glycol Chitosan Hydrogels for
1321 Cartilage Repair, Advanced Healthcare Materials 12(32) (2023) 2302078.
1322 [42] L. Chang, Y. Xu, Z. Wu, Y. Shao, D. Yu, W. Yang, L. Ye, X. Wang, B. Li, Y. Yin,
1323 Hyaluronic acid methacrylate/laponite hydrogel loaded with BMP4 and maintaining its
1324 bioactivity for scar-free wound healing, Regenerative Biomaterials 10 (2023) rbad023.
1325 [43] T.S. Anirudhan, S.S. Nair, A.S. Nair, Fabrication of a bioadhesive transdermal device
1326 from chitosan and hyaluronic acid for the controlled release of lidocaine, Carbohydrate
1327 Polymers 152 (2016) 687-698.

1328 [44] E. Tsanaktsidou, O. Kammona, C. Kiparissides, On the synthesis and characterization of
1329 biofunctional hyaluronic acid based injectable hydrogels for the repair of cartilage lesions,
1330 European Polymer Journal 114 (2019) 47-56.
1331 [45] C. Buckley, T.R. Montgomery, T. Szank, B.A. Murray, C. Quigley, I. Major, Modification
1332 of hyaluronic acid to enable click chemistry photo-crosslinking of hydrogels with tailorable
1333 degradation profiles, International Journal of Biological Macromolecules 240 (2023) 124459.
1334 [46] N. Wang, M. Bora, S. Hao, K. Tao, J. Wu, L. Hu, J. Liao, S. Lin, M.S. Triantafyllou, X.
1335 Li, Hyaluronic Acid Methacrylate Hydrogel-Modified Electrochemical Device for Adsorptive
1336 Removal of Lead(II), Biosensors, 2022.
1337 [47] A. Indurkar, K. Rubenis, A.R. Boccaccini, J. Locs, Development of nanocomposite
1338 hydrogel using citrate-containing amorphous calcium phosphate and gelatin methacrylate,
1339 Frontiers in Bioengineering and Biotechnology 12 (2024).
1340 [48] L. Zhang, H. Jiang, Z. Hu, Concentration-Dependent Effect of Nerve Growth Factor on
1341 Cell Fate Determination of Neural Progenitors, Stem Cells and Development 20(10) (2011)
1342 1723-1731.
1343 [49] J. Wang, J. Yang, P. Gu, H. Klassen, Effects of glial cell line-derived neurotrophic factor
1344 on cultured murine retinal progenitor cells, Mol Vis 16 (2010) 2850-66.
1345 [50] J. Yang, C. Yang, C. Liu, T. Zhang, Z. Yang, Paradoxical effects of VEGF on synaptic
1346 activity partially involved in notch1 signaling in the mouse hippocampus, Hippocampus 26(5)
1347 (2016) 589-600.
1348 [51] H. Hu, W. Yang, Q. Zeng, W. Chen, Y. Zhu, W. Liu, S. Wang, B. Wang, Z. Shao, Y.
1349 Zhang, Promising application of Pulsed Electromagnetic Fields (PEMFs) in musculoskeletal
1350 disorders, Biomedicine & Pharmacotherapy 131 (2020) 110767.
1351 [52] W.-H. Hei, S.-H. Byun, J.-S. Kim, S. Kim, Y.-K. Seo, J.-C. Park, S.-M. Kim, J.W. Jahng,
1352 J.-H. Lee, Effects of electromagnetic field (PEMF) exposure at different frequency and

duration on the peripheral nerve regeneration: in vitro and in vivo study, International Journal of Neuroscience 126(8) (2016) 739-748.

[53] B.M. Maciejewska, J.K. Wychowaniec, M. Wozniak-Budych, L. Popenda, A. Warowicka, K. Golba, J. Litowczenko, Z. Fojud, B. Wereszczynska, S. Jurga, UV cross-linked polyvinylpyrrolidone electrospun fibres as antibacterial surfaces, Sci Technol Adv Mater 20(1) (2019) 979-991.